COMBINATORIAL STUDY OF HYDROGEN STORAGE ALLOYS

A THESIS SUBMITTED TO
THE GRADUATE SCHOOL OF NATURAL AND APPLIED SCIENCES
OF
MIDDLE EAST TECHNICAL UNIVERSITY

BY

RABİA ÖLMEZ

IN PARTIAL FULFILLMENT OF THE REQUIREMENTS
FOR
THE DEGREE OF MASTER OF SCIENCE
IN
METALLURGICAL AND MATERIALS ENGINEERING

MAY 2009

Approval of the thesis:

COMBINATORIAL STUDY OF HYDROGEN STORAGE ALLOYS

submitted by **RABİA ÖLMEZ** in partial fulfillment of the requirements for the degree of **Master of Science in Metallurgical and Materials Engineering, Middle East Technical University** by,

Prof. Dr. Canan Özgen _____
Dean, Graduate School of **Natural and Applied Sciences**

Prof. Dr. Tayfur Öztürk _____
Head of Department, **Metallurgical and Materials Engineering**

Prof. Dr. Tayfur Öztürk _____
Supervisor, **Metallurgical and Materials Engineering, METU**

Examining Committee Members:

Prof. Dr. Vedat Adeniz _____
Metallurgical and Materials Engineering, METU

Prof. Dr. Tayfur Öztürk _____
Metallurgical and Materials Engineering, METU

Prof. Dr. Kadri Aydınol _____
Metallurgical and Materials Engineering, METU

Dr. M. Süha Yazıcı _____
Director, Fuel Cell Technology&Education International
Centre for Hydrogen Energy Technologies, UNIDO-ICHET

Dr.H. Emrah Ünalan _____
Metallurgical and Materials Engineering, METU

Date: 04. 05. 2009

I hereby declare that all information in this document has been obtained and presented in accordance with academic rules and ethical conduct. I also declare that, as required by these rules and conduct, I have fully cited and referenced all material and results that are not original to this work.

Name, Last name: Rabia Ölmez.

Signature:

ABSTRACT

COMBINATORIAL STUDY OF HYDROGEN STORAGE ALLOYS

Ölmez, Rabia

M. Sc., Department of Metallurgical and Materials Engineering

Supervisor : Prof. Dr. Tayfur Öztürk

May 2009, 68 pages

A combinatorial study was carried out for hydrogen storage alloys which involve processes similar to those normally used in their fabrication. The study utilized a single sample of combined elemental (or compound) powders which were milled and consolidated into a bulk form and subsequently deformed to heavy strains. Material library was obtained in a post annealing treatment carried out at elevated temperatures which brings about solid state reactions between the powders yielding equilibrium phases in the respective alloy system. A sample comprising the material library was then pulverized and screened for hydrogen storage composition. X-ray diffraction was used as a screening tool, the sample having been examined both in as-processed and hydrogenated state. The method was successfully applied to Mg-Ni, and Mg-Ni-Ti yielding the well known Mg_2Ni as the storage composition. It is concluded that partitioning of the alloy system into regions of similar solidus temperature would be required to enrich the material library.

Key words: Combinatorial Approach, Hydrogen Storage, Equal Channel Angular Pressing (ecap), Temperature Programmed Sorption, Mg-Ni, Mg-Ni-Ti, Mg_2Ni, $MgNi_2$.

ÖZ

HİDROJEN DEPOLAYICI FAZLARIN HIZLI TAYİNİ İÇİN YÖNTEM GELİŞTİRİLMESİ

Ölmez, Rabia

Yüksek Lisans, Metalurji ve Malzeme Mühendisliği Bölümü

Tez Yöneticisi : Prof. Dr. Tayfur Öztürk

Mayıs 2009, 68 sayfa

Bu çalışma hidrojen depolayıcı fazların tayinine yönelik hızlı bir yöntemin geliştirilmesini konu almaktadır. Çalışma hidrojen depolayıcı mazlemelerin üretiminde de kullanılan süreç ve teknikleri esas almakta ve bu şekilde tespit edilecek kompozisyonların rahatlıkla üretimine olanak sağlamaktadır. Yöntem element ya da bileşik haldeki tozların eşit hacimli olarak harmanlanmasını, toz metalurjisi yöntemleri ile sıkıştırılmasını ve takiben eş eksenli açısal presleme (ECAP) ile aşırı yoğrunmasını esas almaktadır. Tek numune içerisinde ilgili alaşım sistemindeki tüm fazlar son bir tavlama işlemi ile tozların iç reaksiyona sokulması ile elde edilmektedir. Takiben elde edilen numune sabit hacimli bir reaktörde hidrojen basıncı altında ısıtılmakta ve basınç-sıcaklık eğrileri kaydedilmektedir. Hidrojen depolayıcı fazın mevcudiyeti basınçta sapmalara neden olmaktadır. Numune içerisinde hangi fazın hidrojenle reaksiyona girdiği X-ışınları kırınım yöntemi ile tespit edilmektedir. Yöntem Mg-Ni ve Mg-Ni-Ti sistemlerine başarıyla uygulanmış ve bu sistemlerde Mg_2Ni bileşiği hidrojen depolayıcı alaşım olarak doğrulanmıştır. Çalışma farklı ergime sıcaklıklı fazlar içeren alaşım sistemlerinde tek numune kullanımının kısıtlarına işaret etmekte ve bu tür durumlarda alaşım sisteminin benzer ergime sıcaklığına sahip bölgelere ayrılması ile birden fazla numunenin gerekli olabileceğini göstermektedir.

Anahtar Kelimeler: Hidrojen Depolama, Eş Eksenli Açısal Pres, Mg-Ni, Mg-Ni-Ti, Mg_2Ni, $MgNi_2$.

ACKNOWLEDGEMENTS

I wish to express my deepest gratitude to my supervisor Prof. Dr. Tayfur Öztürk for his guidance, advice, criticism, encouragements and insight throughout the research.

I would also like to thank Prof. Dr. Vedat Akdeniz for his suggestions and comments and for production of samples used in this work.

Help and support all of Metal Hydrogen research group members, especially Ms. Gülhan Çakmak, and the technical assistance of Mr. Cengiz Tan in the Metallurgical and Materials Engineering Department as well as Mr. Ünal Pehlivan of LAMASAN are gratefully acknowledged.

Finally, I would like to thank to all my family members for their continuous support and patience.

This study was supported by FP6 NESSHY (Novel Efficient Solid Storage for Hydrogen) Project which I gratefully acknowledge.

TABLE OF CONTENTS

CHAPTER 1

INTRODUCTION

Hydrogen is viewed as a new energy source for the future economy and it is widely believed that it will become the fuel for portable applications within a few decades. It is therefore essential to develop practical and viable hydrogen storage materials before this new form of energy can be commercially used.

To find the storage material, a large number of studies have been carried out and hydrogen storage characteristics of various metallic compositions have been characterized. Typically such studies require a lengthy preparation of specific composition, its processing and the characterization to establish its sorption properties. Not all such studies are successful for end purposes. Before detailed investigations are carried out, a rapid method to identify storage compositions would be highly beneficial. This so called "combinatorial approach" involves the preparation of a sample with multiple alloy compositions (the so-called material libraries) and then studying/screening their storage properties simultaneously.

In this study, combinatorial method is developed based on solid state synthesis of multiple alloy compositions and screening of these using X-ray diffraction technique. The systems under study are Mg-Ni binary and Mg-Ni-Ti ternary systems.

CHAPTER 2

LITERATURE REVIEW

2.1 Combinatorial Material Science

Combinatorial method involves the production of a sample with multiple alloy compositions and then screening them for a particular property simultaneously.

This approach is similar to human immune system which to fight an invading virus, the system generates 10^{14} antibody molecules simultaneously to identify the one that is effective against the virus, (Xiang et al. 1995). Examples of combinatorial studies include peptide synthesis, (Geysen et al. 1984), design of new biocatalysts, glycoprotein ligands synthesis, (Palanisamy et al. 2005), etc.

Applications of combinatorial approach in material science include such topics as phase diagram determination (Boettcher et al. 1955, Zhao 2006, Xiang et al. 1995), superalloy development (Zhao et al. 2001), and determination of flux compositions (Takahashi et al. 2006). The other applications include luminescent materials (Kubota et al. 2004), superconductivity (Hanak et al. 1971), magnetic (Kulkarnı et al. 2006), ferro magnetic (Takeuchi et al. 2003) and dielectric (Chang et al. 2002) material developments.

The combinatorial approach involves i)preparation of a sample with multiple alloy compositions (materials libraries) and then ii) studying/ screening of these compositions with regard to a specific property. A variety of methods have been used in preparing the “materials library”; thin films, diffusion couples, methods based on powder processing, and local melting of compositionally different couples.

Thin film deposition is the most frequently used method in preparing the material library. Boettcher et al. (1955) have used this method to determine phase diagram of Ag-Sn, Au-Sn, Ag-Pb-Sn systems. A similar study was carried out by Kenedy et al. (1965) for Cr-Ni-Fe system. In this study elements were evaporated simultaneously from different sources by EB-PVD and deposited onto a heated substrate in such a way that the composition of the deposit varies from point to point.

Hanak (1971) worked on co-sputtered thin film samples of superconductor materials. For thin film sample preparation a sputtering module with a target electrode and a substrate holder were used. The target was composed of half disks of two different materials for binary and 120° sections of three different materials for ternary systems. A strip substrate and disk shape substrate were used for binary and ternary systems respectively. Co-sputtering was performed using a single source which similar sputtering rates for different elements. In the end, co-sputtered thin films had composition profiles varied as a function of position on the substrate.

Xiang et al. (1995) have used a physical masking technique to prepare material libraries in thin film samples. They were generated by sputtering the target onto physically masked substrates, i.e. elements were sputtered in turn and deposited on the unmasked regions while the masked regions were protected from film deposition. Alternative masking geometries were used to produce different compositions on the substrate. Samples were as small as 200 X 200 micrometers in size yielding density values for materials library as high as 10000 sites per square inch.

Takahashi et al. (2006) in developing flux material for liquid phase mediated epitaxy of $Bi_4Ti_3O_{12}$ single crystal film have used pulsed laser deposition technique. For this purpose, both $Bi_4Ti_3O_{12}$ and candidate material for flux were prepared by solid state reaction of the constituent oxides. At first, the flux library

was deposited on a $SrTiO_3$ substrate by laser deposition and then a stiochiometric $Bi_4Ti_3O_{12}$ film was deposited onto this library. The growth of $Bi_4Ti_3O_{12}$ thin film was checked to find the suitable flux composition within the thin film material library.

Bulk methods were also used in preparing samples for combinatorial studies. Hasebe et al. (1978) and Jin (1981) used this method for construction of phase diagrams. To form junctions diffusion couples or multiples were produced by placing bulk elements. In this way different phases were formed through inter-diffusion of elements in intimate contact with one another. The local equilibrium at the phase interfaces allowed forming composition profiles and phasing diagram isotherms. Similar approach was used by Zhao et al. (2001) for development of superalloys.

Local melting can also be used to develop different phases in alloy systems. Cohen et al. (1999), using this technique, studied Al-Co to discover the possible compounds in this system. In this study, pointed rods were placed in contact with each other and were locally melted in the tip. This is followed by freezing to form compounds in the alloy system.

Bulk samples can also be produced by powder metallurgy. Such a study was reported by Akyıldız et al. (2004, 2007). This study was based on mechanical milling of elemental powders under protective atmosphere followed by hot compaction and sintering. Also Yang et al. (2004) have developed a multi-component powder dispensing system which allows the preparation of samples with composition gradient.

For screening of material libraries or regions with compositional gradients a variety of techniques were used. Boettcher et al. (1955) in constructing the phase diagram have used electron diffraction to identify and characterize the phases. Similarly Kenedy et al. (1965) have used combined methods of X-ray

fluorescence (XRF), X-ray diffraction (XRD) and electron probe microanalysis (EPMA) techniques for the same purpose. In addition, optical microscopy and microprobe analysis techniques have been used by Cohen et al. (1999) again for phase diagram study.

Zhao (2001) have used micro-mechanical testing as a screening method to characterize the mechanical properties such as hardness and elastic modulus of superalloys. For superconductivity, Xiang et al. (1995) have used four point probe technique to measure the resistance of superconductor material libraries. Takahashi et al. (2006) have used microspot X-ray technique to screen the crystallinity in the growth of thin film.

2.2 Combinatorial Study of Hydrogen Storage Alloys

Combinatorial studies for hydrogen storage alloys are relatively new. First reports were made in 2003 by Olk et al.(2003), Akyıldız et al. (2004) and Zhao et al. (2004). The former study was based on the thin film and the latter two were based on bulk method.

Akyıldız et al. (2004, 2007) have used powder technique to fabricate a multiphase sample in Mg-Al system and screened this using XRD. In this study, the sample was hydrided in a Sievert's type apparatus, pressure change being monitored as the sample was heated up. Pressure drop was taken as the sign of the presence of a hydrogen storage phase in the sample.

Zhao et al. (2004) have used diffusion couples for combinatorial study of hydrogen storage alloys. They selected 15 elements and, material libraries have been produced by solid state reaction of diffusion couples in their contact regions. Time-of -flight secondary ion mass spectroscopy has been used as a screening tool.

Olk et al. (2003) for their study on the combinatorial method have used thin

films of Mg-Ni-Fe ternary and Mg-Ni binary systems. They synthesized the thin films using a combination of magnetron sputtering and pulsed laser deposition techniques. As a screening tool they used infrared camera as a way of detecting temperature changes caused by hydriding/dehydriding. The method worked well for most cases but there were difficulties associated with experiments conducted at temperatures close to room temperature. This method was further developed by Dam et al. (2007) who overcome this difficulty using optical transmission of the visible part of the optical spectrum rather than the thermal emissivity. The new method has been used successfully in Mg-Ni-Ti where the phases involved change their optical state upon hydriding and dehydriding.

2.3 Hydrogen Storage in Mg-Ni-Ti System

Hydrogen storage in Mg-Ni-Ti will be reviewed first for the constituent elements, then for the binary and finally for the ternary system.

2.3.1 Magnesium

Magnesium (Mg) is a well known hydrogen storage element with 7.6 wt % storage capacity, Pedersen et al. (1983). It has hexagonal crystal structure in the elemental form, but converts to tetragonal structure when it is hydrided. The binary phase diagram of Mg-H is given in Figure 2.1(Manchester et al. 1988). The hydrogenation takes place via a primary dissolution of H in Mg. Maximum solubility of H in Mg (α) is 9.1 at. %. More dissolution of H in Mg(α) lead to MgH_2 (β) compound formation. The crystal and lattice parameter details of Mg and its hydride are given in Table 2.1. The enthalpy of hydride formation is -75 kJ/mole-H_2, (Pedersen et al. 1983). Pressure-composition-temperature (PCT) diagram Mg is given in Figure 2.2 (Manchester et al. 1988). Although Mg has a high storage capacity, its sorption properties are problematic. As shown by Huhn et al. (2005), Bogdanovic et al. (1999) and Zaluska et al. (1999) both absorptionand desorption of Mg requires quite high temperatures (350–400°C). Moreover the reaction rate at these temperatures is very slow. To overcome

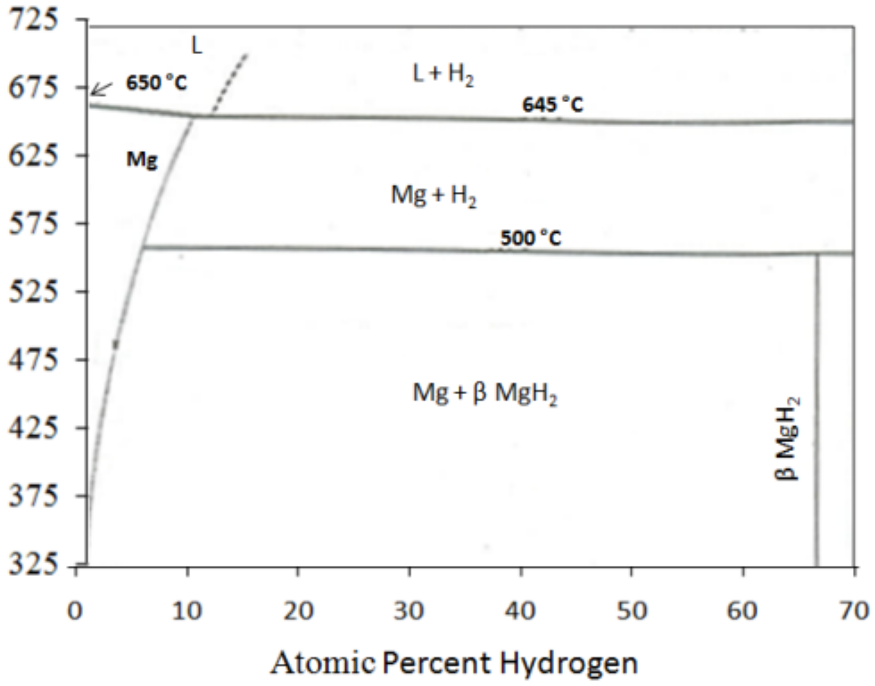

Figure 2. 1 Phase diagram of Mg-H system, Manchester et al. (1988).

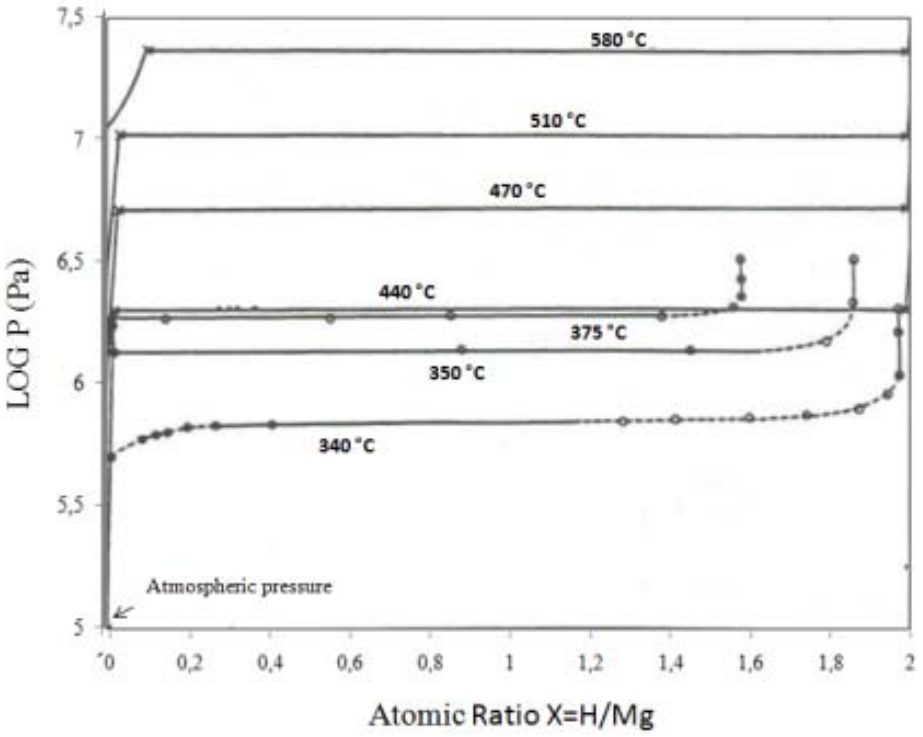

Figure 2. 2 Pressure-composition-temperature diagram of Mg-H system, Manchester et al.(1988)

these problems, Mg powders were often mechanicaly milled with some additives to refine the powders to extremely small sizes. Schluz et al. (1999) was one of the first who mechanically milled Mg and concluded that the milled powders have better sorption properties than unmilled Mg. Similar studies were performed by Zaluska et al. (1999) and Orimo et al. (2001).

In order to further improve the sorption properties of Mg, elements such as Pd (Zaluska et al. 1999, Yermakov et al. 2006), Ni (Liang et al. 1999, Varin et al. 2007, Jensena et al. 2006), Ti (Liang et al. 1999), Fe (Liang et al. 1999, Yermakov et al. 2006), Mn (Liang et al. 1999), V (Zaluska et al. 1999, Liang et al. 1999, Güvendiren et al. 2004), Zn (Zaluska et al. 1999), Y (Zaluska et al. 1999), Cu (Yermakov et al. 2006), Graphite (Imamura et al. 2002, Güvendiren et al. 2004) have been added as additives to Mg. Ni was a commonly used additive for Mg in many studies Varin et al. 2007, Jensena et al. 2006, etc. Varin et al. 2007 and Jensena et al. 2006 have added Ni in different fractions and sizes by mechanical milling. Addition of Ni (0. 5- 2 wt. %) has increased the rate of hydrogen absorption as compared to pure Mg. Moreover, addition of Ni to the mechanosynthesized MgH_2 reduced its hydrogen desorption temperature by 30–50 °C with respect to pure MgH_2 powder. These and other similar studies showed that alloying of Mg with Ni improved the hydriding/dehyriding kinetics and reduced the desorption temperature of Mg.

In addition to elemental additions, some oxides such as V_2O_5 (Yermakov et al. 2006), Nb_2O5 (Friedrichs et al. 2006, Barkhordarian et al. 2004), Al_2O_3 (Güvendiren et al. 2004, Friedrichs et al. 2006), also SiC (Güvendiren et al. 2004), VH_2 (Yermakov et al. 2006, Güvendiren et al. 2004) and NiPd (Yermakov et al. 2006) compounds have also been added to Mg.

Both elemental and oxide additives have been found to have a positive effect onthe sorption kinetics. However, the sorption temperatures of Mg were little

affected by these additions. The lowest desorption temperature reported for Mg is about 280°C (Klassen et. al. 2006).

Table 2. 1 The crystal and lattice parameter details of Mg-H system, Manchester et al. (1988)

Phase	Crystal Structure	Person Symbol	Proto-type	Lattice a, nm	Lattice b, nm	Lattice c, nm
Mg	HCP	hP2	Mg	0. 32093	-	0. 52107
Mg(α)						
MgH_2 (β)	Tetragonal	tP6	TiO_2 (rutile)	0. 45168	-	0. 30205

2.3.2 Titanium

Titanium (Ti) has a storage capacity of 4 wt %. It has hexagonal crystal structure (α) at low temperatures. Above 880°C, Ti transforms to body centered cubic (β) structure. The phase diagram of Ti-H is given in Figure 2.3 (Okamoto 1992). As determined from the phase diagram, maximum amount of H that can be dissolved in Ti (α) is 8 at % which occurs at the eutectoid temperature. Ti (β) phase which forms above the eutectoid temperature dissolves up to 50 at% of H at 833 °C. Further dissolution of H in Ti (β) cause the formation of TiH_2 (β) phase. The compound TiH_2 (β) has a face centered cubic (fluorite type) structure. Below -95°C, TiH_2 (β) transforms to TiH_2 (α) phase. Crystal structures and lattice parameters of hydrides as well as pure phases are given in Table 2.2.

Hydrogenation of Ti occurs readily even under low H_2 pressures. Its enthalpy of formation is -144 kj/mole-H_2 (Fact, 2008). Decomposition temperatures are quite high, 650°C, (Zaluska et al. 2006). PCT diagram of Ti-H system at 629°C and 578°C are given in Figure 2.4 (Mueller et al. 1968).

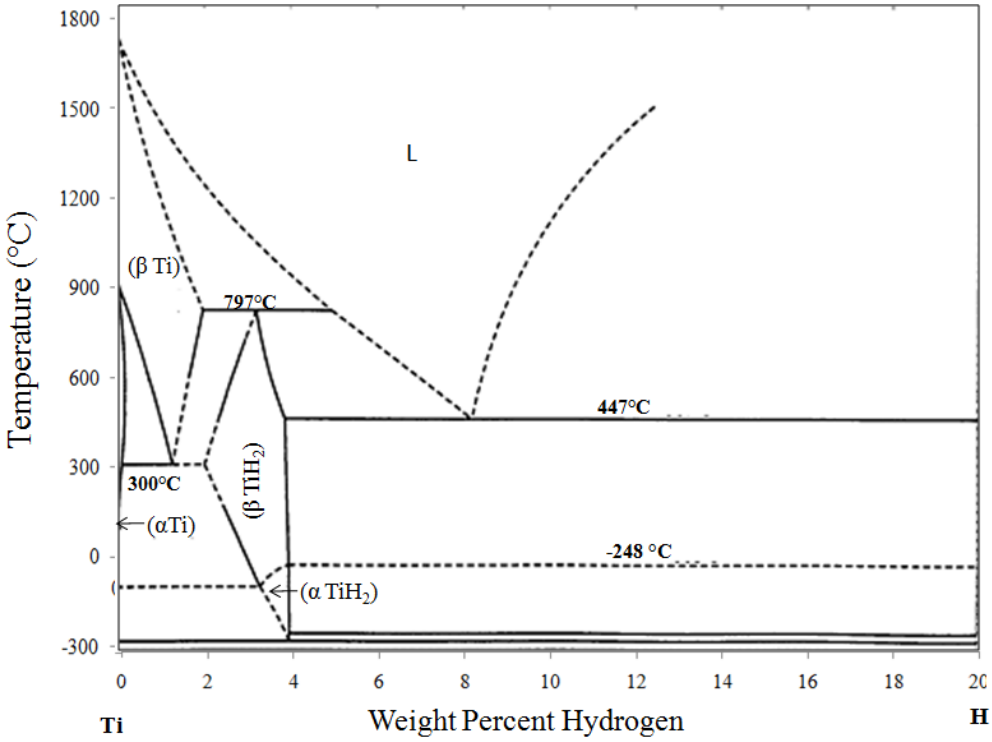

Figure 2. 3 Phase Diagram of Ti-H, Okamoto (1992)

Table 2. 2 The Crystal and lattice parameter details of Ti-H system, *Cullity (1998), **Kulikov (1985), ***Malov et al. (1994)

Phase	**Crystal Structure**	**Person Symbol**	**Proto-type**	**Lattice a,nm**	**Lattice b,nm**	**Lattice c,nm**
Ti(α)	HCP	hP2	Mg	0. 29512*	-	0. 46845*
Ti(β)	BCC	cI2	W	0.33066*	-	-
TiH_2(β)	FCC	cF12	CaF_2	0. 45345***	0. 45345***	0. 45345***
TiH_2(α)	Tetragonal	t16	ThH_2	0. 320**	0. 320**	0. 428**

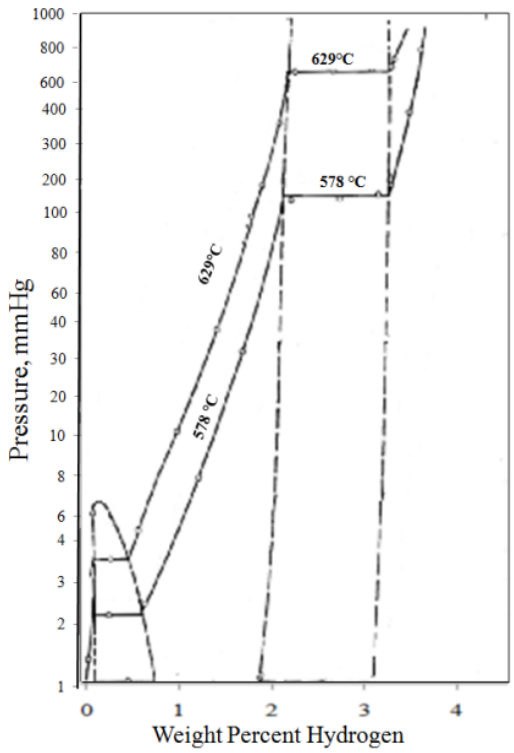

Figure 2. 4 Pressure-composition-temperature diagram of Ti-H system at 629°C and 578°C, Mueller et al. (1968)

2.3.3 Nickel

Nickel (Ni) has a face centered cubic (FCC) crystal structure. When it is hydrided, H atoms are situated in the octahedral interstices of the FCC lattice. The structure remains as FCC with expanded lattice; Ni with 0.3524 nm, its hydride lattice with 0.3721 nm. Thus the hydride expands 5.5 %. The hydride phase however is quite unstable; its formation enthalpy is +39kj/mole-H_2 (Fact, 2008). At room temperature it decomposes totally after 40 hr (Mueller et al. 1968).

2.3.4 Binary Mg-Ni System

Binary phase diagram of Mg-Ni is given in Figure 2.5 (Nayeb-Hashemi et.al. 1985). As can be seen from the phase diagram Mg and Ni have no solubilities in

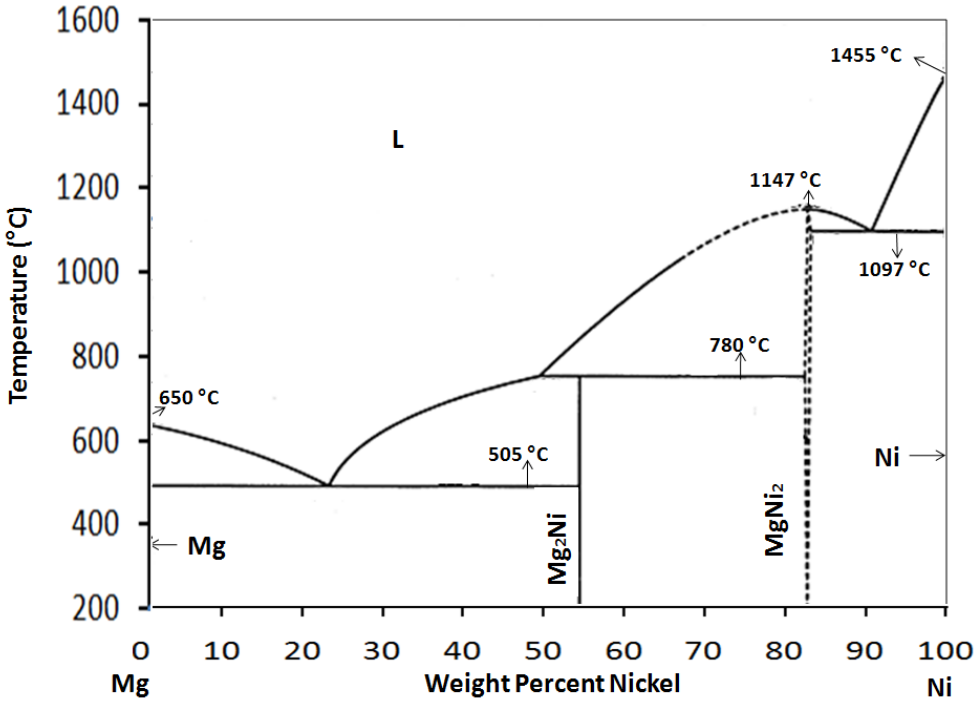

Figure 2. 5 Phase diagram of Mg-Ni system, Nayeb-Hashemi et.al. (1985)

Table 2. 3 The crystal and lattice parameter details of Mg-Ni and Mg-Ni-H systems, *Buschow (1975), **Haussermann et al. (2002), ***Yvon et al. (1981)

Phase	**Crystal Structure**	**Person Symbol**	**Proto-type**	**Lattice a,nm**	**Lattice b,nm**	**Lattice c,nm**
Mg_2Ni	HCP	hP18	Mg_2Ni	0. 5212*	0. 5212*	1. 3247*
Mg_2NiH_4(LT)	Monoclinic			1. 4343**	0. 64038**	0. 64830**
Mg_2NiH_4(HT)	FCC	cF12	CaF_2	0,6490***	-	-
$MgNi_2$	HCP	hP24	$MgNi_2$	0. 4833*	0. 4833*	1. 5855*

each other. The system comprises of two intermetallic phases, Mg_2Ni and $MgNi_2$. Ni has been used extensively an additive for Mg, (Liang et al. 1999). Mg_2Ni is the well known hydrogen storage alloy. It absorbs up to 3. 6 wt % hydrogen and has better kinetic properties than that of pure Mg (Reilly et al. 1968). The enthalpy of hydride formation is -65 kJ/mole-H_2 (Fact, 2008). Mg_2Ni intermetallic phase could be synthesized with a variety of methods; e.g mechanical alloying under Ar or H_2 gas (Orimo et al. 1997, Janot et al. 2004, Vijaya et al. 2005); bulk mechanical alloying (Aizawa et al. 1999); combustion synthesis (Saita et al. 2002) and melting (Bystrzycki et al. 2003).

The intermetallic Mg_2Ni has hexagonal crystal structure (hP18). It hydrides to Mg_2NiH_4 which is monoclinic at room temperature, Table 2.3. Yvon et al. (1981) reports that the monoclinic Mg_2NiH_4 is subject to a phase transition at 245°C which converts it to cubic Mg_2NiH_4. In the latter structure, Mg ions form a cube around the NiH_4 complex, building an anti-fluorite type structure (Yvon et al. 1981). According to Blomovist et al. (2003), room temperature monoclinic structure, has two XRD peaks (Cu Kα) in $\sim 23° < 2\theta < 24°$. Above the transition temperature these two peaks disappear and a single peak at $2\theta = 23.7°$ occurs which is consistent with the cubic structure. Ronnebro et al. (1999) have that shown that it is possible to convert monoclinic Mg_2NiH_4 to cubic structure by mechanical milling at room temperature.

Similar to pure Mg, a number of studies have been carried out to improve the hydrogen storage properties of Mg_2Ni phase via mechanical milling and by the use of additives. Vijay et al. (2005) have mechanically milled the elemental powders of Mg and Ni in a ratio of 2:1 under Ar and characterized its sorption properties. It has been shown that Mg_2Ni phase which forms as result of milling could absorb hydrogen to its nearly full capacity at 250°C. A similar study has been carried out by Orimo et al. (1997). Janot et al. (2004) have used Pd and graphite as additives during milling of the elemental powders and the resulting Mg_2Ni phase displayed storage capacity of 2.7 wt% at 150 °C.

The other intermetallic in Mg-Ni system, $MgNi_2$ does not absorb hydrogen. Kusedome et al. (2007) have subjected $MgNi_2$ phase to severe plastic deformation via high pressure torsion and investigated its hydrogenation behavior. It has been found that the intermetallic could store 0.1 wt% hydrogen at 100°C. Hatano et al. (2002) have attempted to hydrogenate $MgNi_2$ by exposing it to atomic hydrogen at elevated temperatures. These studies confirmed the fact that $MgNi_2$ phase is not of practical interest as hydrogen storage alloy.

2.3.5Binary Mg-Ti Sytem

Phase diagram of Mg-Ti system is given in Figure 2.6 (Nayeb-Hashemi et.al.1998). The elements have no solubility in each other, also there are no intermetallic compounds. A number of studies have been carried out for Mg-Ti binary system. Vermeulen et al. (2006) have used electron-beam deposition to produce metastable alloys. It has been found that in this way, crystalline phase of Mg alloys containing up to 20 at.% Ti could be synthesized. This alloy, $Mg_{80}Ti_{20}$ had a superior reversible hydrogen storage capacity of 6 wt % H, Vermeulen et al. (2007). Furthermore it has been found that the doping of Mg with Ti has positively affected the kinetics of hydrogenation compared to pure Mg. The single phase Mg alloys produced in this way have FCC-structure after hydrogenation.

In a similar study, Germaud et al. (2007) have produced Mg thin films doped with Ti. It has been found that hydrogenated film with alloy compositions between $Mg_{65}Ti_{35}$ and $Mg_{86}Ti_{14}$ has FCC structure. However, enthalpy of these hydrides were found to differ little (-65kJ/mol-H2) from that of rutile MgH_2. The enthalpy in thin films incorporating less than 14 at % Ti however was -61 kJ/mol-H_2 which is less than that of pure MgH_2. This shows that Mg-Ti hydrides could be less stable than pure MgH_2. The authors have reported that the Mg-Ti compositions mentioned above have good optical switching properties and excellent hydrogenation kinetics.

Liang et al. (2003) have synthesized Mg-Ti alloys via mechanical alloying. It has been shown that as a result of milling, 12.5 at % Ti could be dissolved in Mg while maintaining its hexagonal structure. This leads to a decrease in the c/a ratio of the crystal lattice. The extended solubility improves the kinetics of hydrogenation. However, capacity and the stability of hydrides were little affected and were compareble to those of Mg. It has been shown that the supersaturated solid solution of Mg-Ti alloy decomposes upon thermal annealing. It is also found that hydrogenation enhances this decomposition. During hydrogenation the single phase alloy has been transformed to MgH_2 and TiH_2. So the incorporation of Ti into Mg was temporary and disappears with the first cycle.

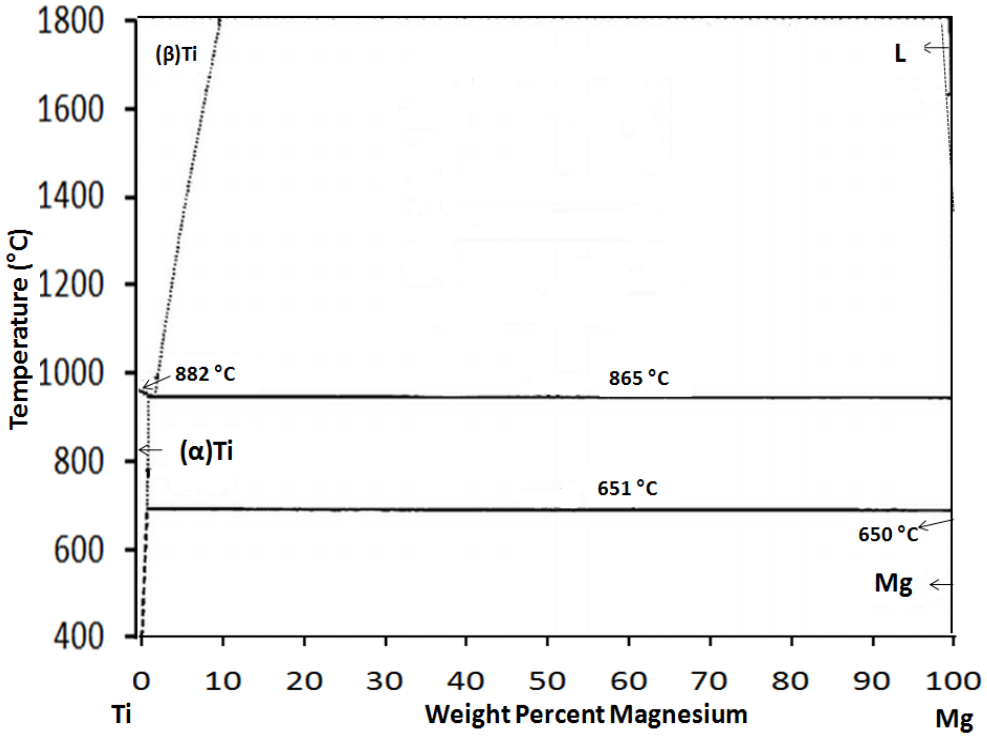

Figure 2. 6 Binary Phase Diagram of Mg-Ti, Nayeb-Hashemi et.al.(1998)

Kyoi et al. (2004) have synthesized Mg-Ti hydride under high H_2 pressure (8 GPa). This hydride, Mg_7TiH_x, as detected with XRD had FCC structure with a=0.47658 nm. It has Ca_7Ge type structure with 5.5 wt % storage capacity. The compound releases its hydrogen at around 332°C by decomposing into Mg and $TiH_{1.9}$ releasing 4.7 mass% of hydrogen (this temperature is lower by 130°C and 220°C as compared to MgH_2 and TiH_2, respectively). As can be understood from this decomposition cycle, no binary Mg-Ti phase exists and the new reported phase exists only as ternary hydride by the support of hydrogen atoms.

2.3.6 Binary Ti-Ni System

Ti-Ni binary has three intermetallic phases: Ti_2Ni, TiNi, $TiNi_3$, Figure 2.7. Ni is soluble in Ti up to 15 at.% whereas Ti has no solubility in Ni. The crystal structure and lattice parameters of the phases are given in Table 2.4. It is known that Ti_2Ni and TiNi could store hydrogen though the amount is not substantial. Hydride of Ti_2Ni is quite stable, Chen et al. (2002).

Table 2. 4 The crystal and lattice parameter details of Ti-Ni and Ti-Ni-H systems,* Takeshita, (2002), ** Schmidt et al.(1989), ***Eskandarany et al. (1995), # Emiliani et al.(1990), ## Noreus et al.(1985), ###Buchner et al.(1972).

Phase	Crystal Structure	Person symbol	Proto-type	Lattice a,nm	Lattice b,nm	Lattice c,nm
Ti_2Ni	FCC	cF96	Ti_2Ni	1.1331*	1.1331	1.1331
TiNi	Cubic	cP2	CsCl	0.3015**	0.3015	0.3015
$TiNi_3$	HCP	hP16	$TiNi_3$	0.510#	-	0.830
$NiTiH_3$	FCC			0.35403***	-	-
TiNiH	Tetragonal			0.6221##	0.6221	1.2363
Ti_2NiH	Cubic		Fe_3W_3C	1.1500###	-	-

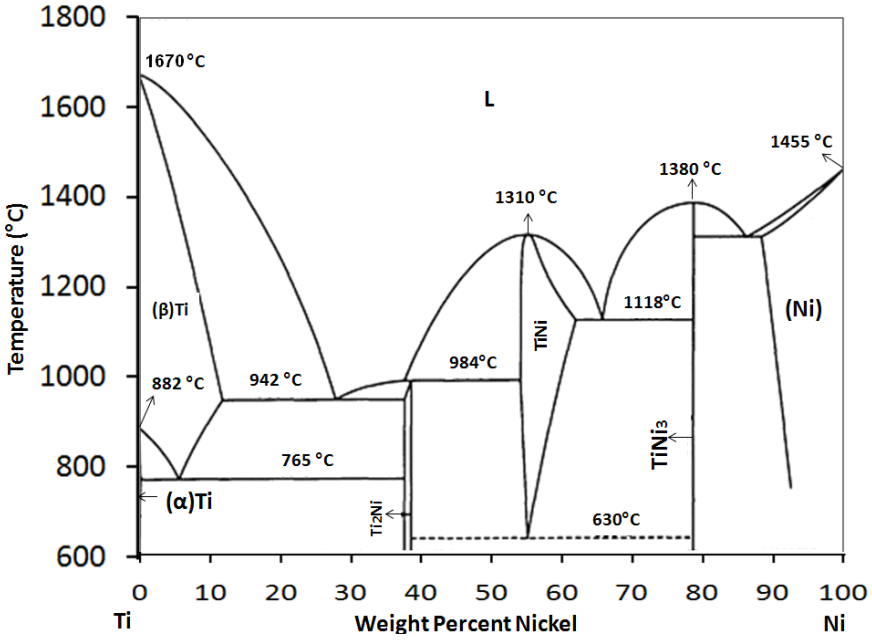

Figure 2. 7 Binary phase diagram of Ti-Ni, Massalski (1990)

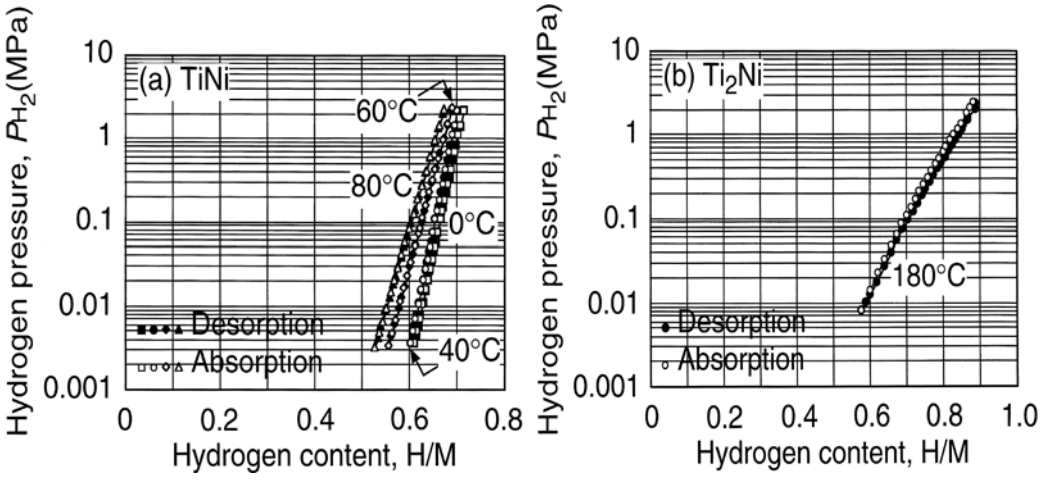

Figure 2. 8 Pressure-composition-temperature diagrams of TiNi and Ti_2Ni, Takeshita et al. (2002)

Takeshita et al. (2000) have synthesized TiNi and Ti_2Ni by arc melting and found that both TiNi and Ti_2Ni have no plateau pressure for both absorption and desorption, Figure 8. It has been reported that the storage capacity, under 20 bar, are 1.3wt % at 80 °C and 1.7 wt% at 180 °C for TiNi and Ti_2Ni respectively. Similar study was carried out by Chen et al. (2002) where the intermetallics were hydrided under 60 bar at 75°C yielding phases TiNiH and Ti_2NiH.

Bobet et. al. (2002) have used mechanical alloying to synthesize Ti-Ni samples. For this purpose elemental powders have been mixed and milled under H_2. This has lead to the formation of TiH_2 while Ni remained unaffected. Subsequent heat treatment at 450°C led to the formation of $TiNiH_{1.4}$. In addition milling of TiNi intermetallic directly under H_2 has yielded the same phase: $TiNiH_{1.4}$. In a similar study Eskandarany et al. (1995) have used equiatomic mixture of Ti-Ni. Under H_2 milling, the initial formatin of TiH_2 was followed by solid solutionizing to $NiTiH_3$. The latter phase is FCC with lattice parameter of a=0.35403 nm.

2.3.7Ternary Mg-Ni-Ti System

Phase diagram of Mg-Ti-Ni ternary is not available. No ternary phase involving elements Mg,Ni,Ti has been reported in the literature. This is except for Mg_3TiNi_2 phase which has been reported by Guangile et al. (2001) (as discussed below).

Ternary mixtures and thin film compositions which have been investigated in Mg-Ni-Ti system have been marked in the ternary diagram are given in Figure 2.9 and Table 2.5. Of these $Mg_{1.7}Ti_{0.3}Ni_{0.8}Mn_{0.2}$ has been studied by Guangile et al. (2001) via mixing the elemental powders. The mixed powders have been compacted and sintered at 540°C, as a result of which Mg_2Ni and $TiNi_3$ binary phases and Mg_3TiNi_2 ternary phase have been synthesized. Guangile et al. (2001) reports that the crystal structure of this ternary phase was cubic with a=1.16178 nm. In a similar study, Sheppard et al. (2006) have mixed elemental

powders corresponding to a composition of $Mg_{47}Ni_{20}Ti_{53}$ and milled them under Ar. This yielded only Ti_2Ni intermetallic as an additional phase. When loaded with H_2, Mg and Ti were hydrided together with Ti_2Ni. The storage capacity of Ti_2Ni was 2.5 wt %. Hong et al. (2002) have prepared the ternary mixtures from elemental powders with compositions of $Mg_8Ti_2Ni_{0.55}$ (Mg_8Ti_2-10wt%Ni) and $Mg_9Ti_1Ni_{1.14}$ (Mg_9Ti_1-20wt%Ni). As a result of milling Mg_2Ni and Ti_2Ni phases were obtained in both mixtures. It has been reported that the total hydrogen absorption capacity of the mixture was 4.5-5.5 wt %.

Liang et al. (1999) and Spassov et al. (2003) have used Mg_2Ni and Ti as starting material and have milled them to replace some of the Mg with Ti. No structural change was observed in Mg_2Ni, though the formation enthalpy of Mg_2Ni was decreased as a result of this processing and its sorption kinetics was improved. An alternative approach in synthesizing the compounds are thin film processing. Griessen et al. (2007), using a combinatorial method, have deposited thin films on quartz or sapphire wafers by means of magnetron sputtering using tilted Mg, Ni and Ti sources that are positioned 120°in a circle around the substrate. The wafer used had a diameter of 75 mm and were placed at a distance which allowed considerable compositional differences. The films were capped with a 20 nm Pd overlayer to promote H_2 dissociation and to prevent oxidation of the underlying film. The wafers were then placed in an optical cell with a heating facility up to 300 °C. The cell was used to follow the hydrogenation behavior of the thin films by monitoring the changes in their optical transmission. The cell transmitted light as a function of the slowly increased hydrogen pressure. The approach was based on the Lambert–Beer's law, according to which the logarithm of the optical transmission is proportional to the local hydrogen concentration. had a diffuse white light source to illuminate the sample from the substrate side, and had a charge coupled device (CCD) camera to continuously monitor the Using this approach Griessen et al. (2007) have deposited Mg-Ni-Ti films with a compositional gradient and have constructed the pressure–composition isotherms for each pixel of the frame.

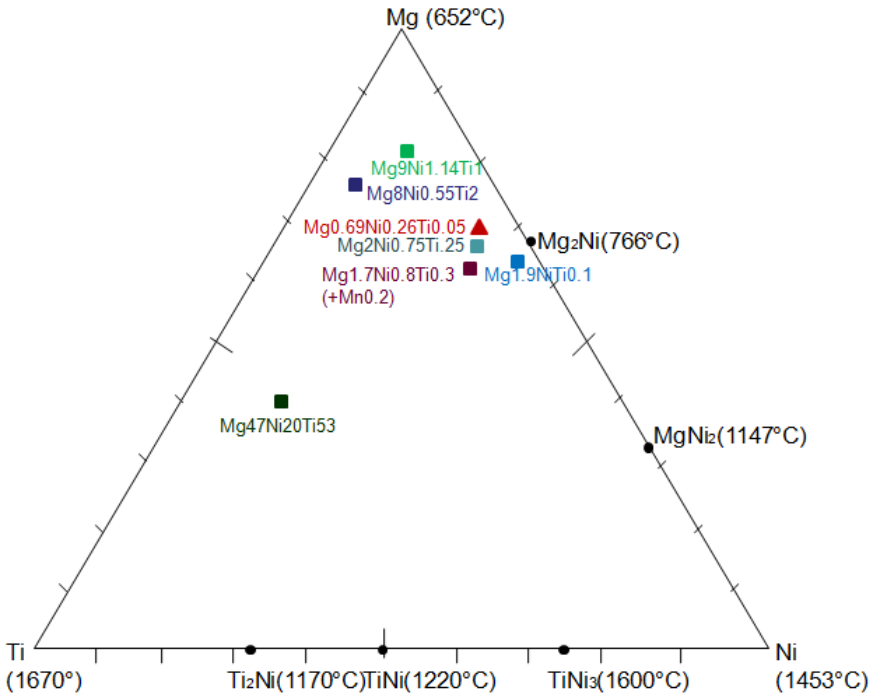

Figure 2. 9 The investigated compositions in Mg-Ni-Ti systems are marked on the ternary system

.

Table 2. 5 The investigated compositions and the sythesized phases in Mg-Ni-Ti

Composition	**Formed Phase(s),**	**Studied by**
$Mg_{1.7}Ni_{0.8}Ti_{0.3}$	Mg_3Ni_2Ti	Guangile et al. (2001)
$Mg_{47}Ni_{20}Ti_{53}$	Ti_2Ni	Sheppard et al. (2007), Lomnes et al. (2002)
$Mg_8Ni_{0.55}Ti_2$	Mg_2Ni, Ti_2Ni	Hong et al.(2002)
$Mg_9Ni_{1.14}Ti_1$	Mg_2Ni, Ti_2Ni	Hong et al. (2002)
$Mg_{1.9}NiTi_{0.1}$	Mg_2Ni	Liang et al. (1999), Spassov et al. (2003)
$Mg_2Ni_{0.75}Ti_{0.25}$	Mg_2Ni	Yang et al. (2002)
Mg-Ni-Ti (thin film)	$Mg_{0.69}Ni_{0.26}Ti_{0.05}$	Griessen et al. (2007)

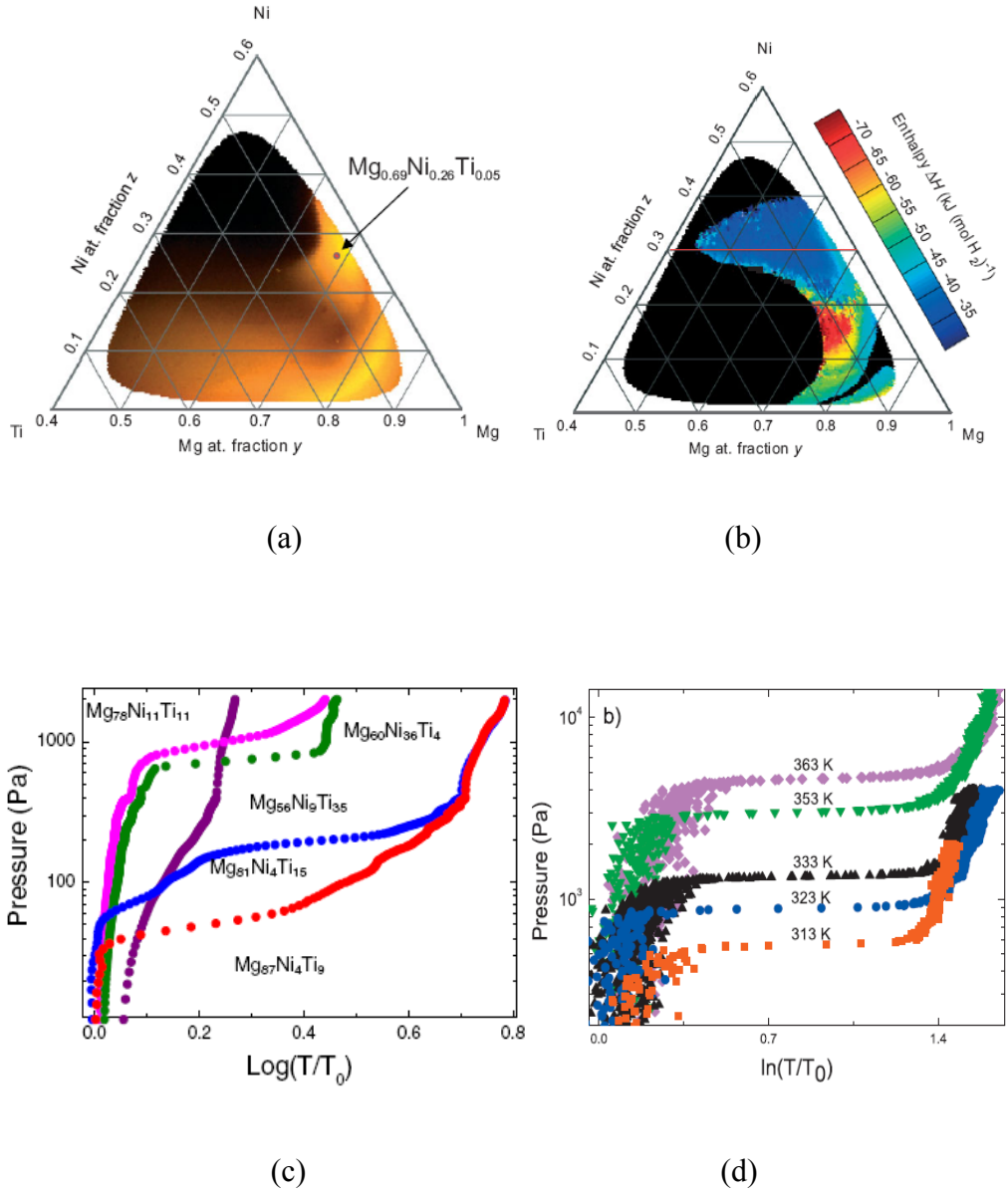

Figure 2. 10 Hydrogenography as applied to Mg-Ni-Ti system (Griessen et al. (2007) and Gremaud et al. (2007))

a) Images of the hydrogen-induced optical transmission during hydrogenation at 60 °C..

b) Processed data collected at a variety of temperature, colors refer to different values of desorption enthalpy.

c) Pressure–optical-transmission isotherms of Mg-Ni-Ti system for different compositions at 60 °C.

d) Pressure–optical-transmission isotherms of $Mg_{69}Ni_{26}Ti_5$ at different temperatures.

The deposited films were x-ray amorphous with a 30-100 nm in thickness. Figure 2.10 (a), (b), (c), (d) are taken from their study which referred to hydrogenation at 60 °C. It is seen that the desorption temperature of hydrides vary depending on the composition. It has been found that quite an extensive range of compositions have the desorption temperature of 60 °C ,i.e. temperature quite suitable for desorption in practical storage applications. The compositions identified are derivatives of the well known composition Mg_2Ni. Of these ,Griessen et al. (2007) have proposed the composition $Mg_{69}Ni_{26}Ti_5$ which has -40kJ/mol-H_2 enthalpy and the storage capacity of 3.2 wt% as a suitable composition for storage purposes. Although the measured enthalpy values refer to thin film samples in hydrogen absorption, Griessen et al. (2007) imly that these enthalpy values would be relevant for hydrogen desorption of all nanostructured materials.

CHAPTER 3

EXPERIMENTAL PROCEDURES

3.1 Materials

Starting materials were elemental powders (Alfa Aesear) of Mg, Ni and Ti. All were provided in ≤ 44μm (-325 mesh) with a purity of 99.8 %. In some experiments (as specified Table 3.1) Ni powders of 10 μm in size and Ti powder of 150 μm in size were used. Scanning Electron Microscope (SEM) images of the starting powders are given in Figure 3.1.

$MgNi_2$ powder was produced from elemental powders via induction melting under Ar atmosphere and cast centrifugally into a Cu block, Figure 3.1 (h), which was then crushed into powder by milling. Energy Dispersive X-ray Analysis (EDS) of as-cast material was Mg-72 at % Ni which indicates the presence of some excess Ni in the structure. The powders were separated into two sizes by sieving; ≥ 44 μm (+325 mesh) and ≤ 44 μm (-325 mesh), Figure 3.1 (e) and (f).

3.2 Processes

A schematic representation of the sample preparation and characterization procedures followed in this study is given in Figure 3.2. Sample preparation followed two routes. In one, alloy or elemental powders were mixed and hot compacted at selected temperatures. In the other, the route involved "granulation", i.e. elemental or alloy powders were processed to a certain size either in the form of granules or layers which were arranged within a Cu mold

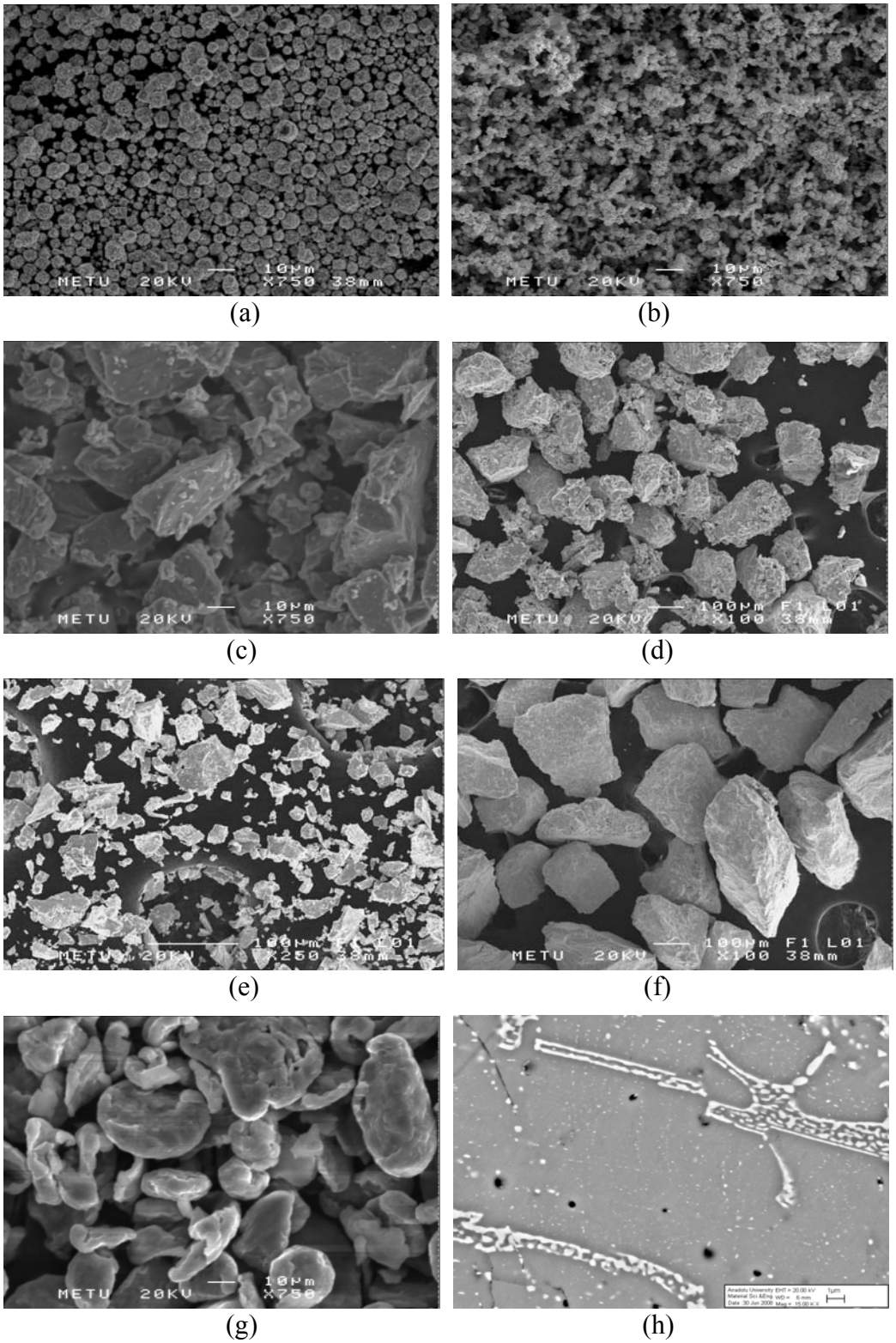

Figure 3. **1** SEM images of starting powders. a) Ni, 10 µm, b) Ni, ≤44µm, c) Ti, ≤44µm, d) Ti, 150 µm, e) $MgNi_2$, ≤ 44 µm , f)$MgNi_2$, ≥ 44 µm g) Mg, ≤44µm, h) Microstructure of $MgNi_2$ casting.

and then compacted via swaging. The difference between the two is the scale of structure.

Samples derived from both routes are then deformed via equal channel angular pressing (ECAP) and subsequently subjected to annealing treatment. Samples which were in bulk form were then milled under Ar atmosphere and consequently subjected to hydrogenation experiment.

Powder Processing: Powders were blended in equal volumetric proportions so as to maximize particle-particle contact. Powders were mixed and in a Spex mill under Ar atmosphere for 15 minutes. Mixed powders were then hot pressed in a metal mould under a pressure of 400 MPa yielding pellets of 8 mm diameter. They were then placed in a Cu block, 14 x14 mm cross section inside a hole, drilled from one end. After placing the pellets, the hole was closed by driving a Cu insert into it, Figure 3.3. Samples embedded in Cu blocks were sintered/annealed at approximately 375 °C under a pressure of 400 MPa.

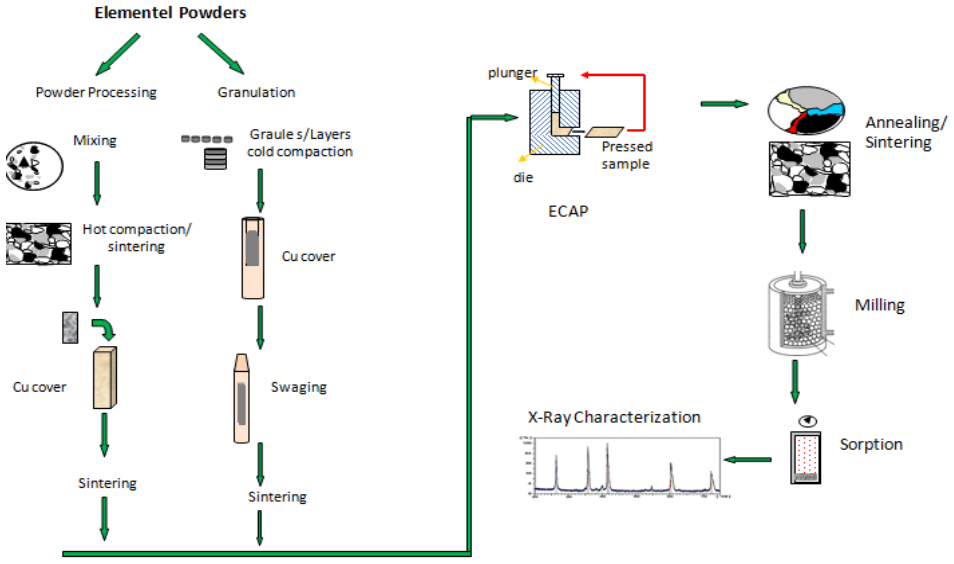

Figure 3. 2 Schematic presentation of combinatorial method to solid state synthesis and screening of hydrogen storage alloys.

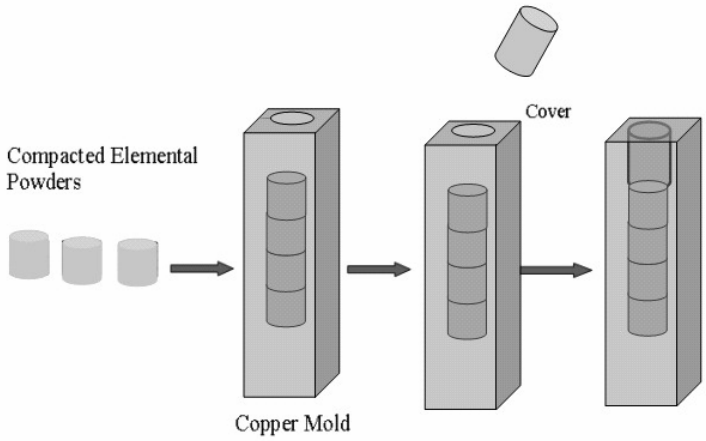

Figure 3. 3 Schematic presentation of powder compacts as they were embedded in a Cu block.

Granulation: Since mixing/milling of powders in elemental form produces a rather fine structure, where needed, a size control was exercised on powders by preprocessing them to a coarser form; two forms were employed for this purpose; one was a layered structure and the other was in the form of granules, Figure 3.4.

For layered structure, alternating layers of metallic powders; Mg and Ni each 2 mm thick loosely pressed compacts were placed one over the other in a mold. They were then compacted at a pressure of 400 MPa yielding cylindrical pellets of 8 mm in diameter and 10 mm in height.

The samples were compacted by swaging in a two stage process. In the first stage, a Cu tube was used which was 22 mm in diameter closed with a rod (18 mm in diameter) by swaging it from one end. Pellets were placed in this tube surrounded by another powder. This was Ni for the binary and Ti for the ternary system, both were compacted in situ. The Cu block with embedded sample was swaged down to 11.5 mm. In the second stage, the swaged sample, which was in bulk form, was removed from the swaged Cu block and was placed inside a new

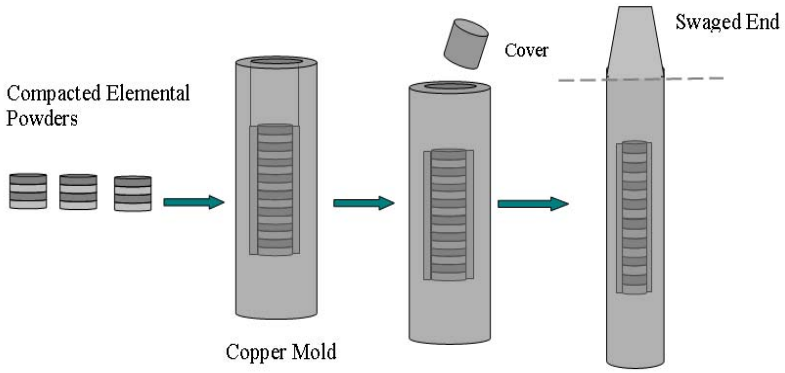

(a)

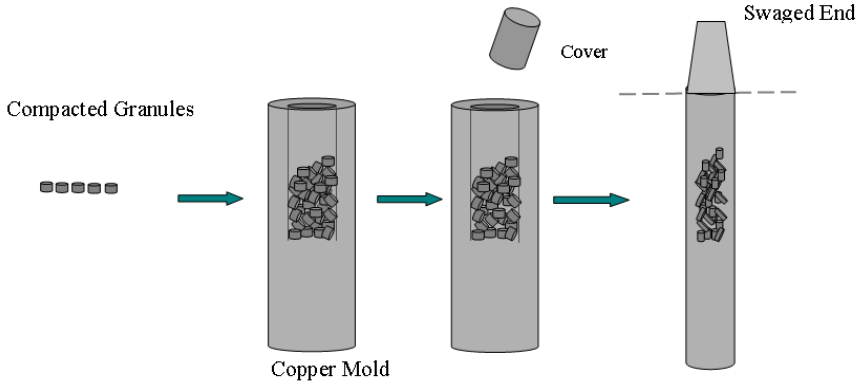

(b)

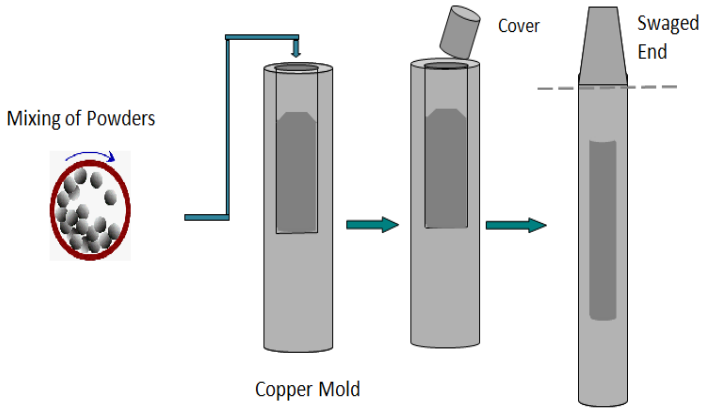

(c)

Figure 3. 4 Sample preparation procedures using, a) alternating layers, b) granules, c) powders.

Cu tube of 22 mm diameter with inner hole of 12 mm closed at one end. The Cu tube with embedded sample was swaged down to 19 mm. They were then sintered/annealed in the furnace at 300 °C before ECAP process. Sintered samples were machined from 19 mm to 18 mm.

For granulation, a special press was constructed with a housing that could be filled with a fixed amount of powders to yield granules of predetermined shape. This is shown in Figure 3.5 (a) and (b). Granules of Mg, Ni, $MgNi_2$ produced in this way were 3 mm in diameter and 2-3 mm in height ,Figure 3.5 (c) and (d). They were then placed in a drilled Cu rod in a random fashion, Figure 3.4 (b). The Cu block was then swaged down to 19 mm as described above.

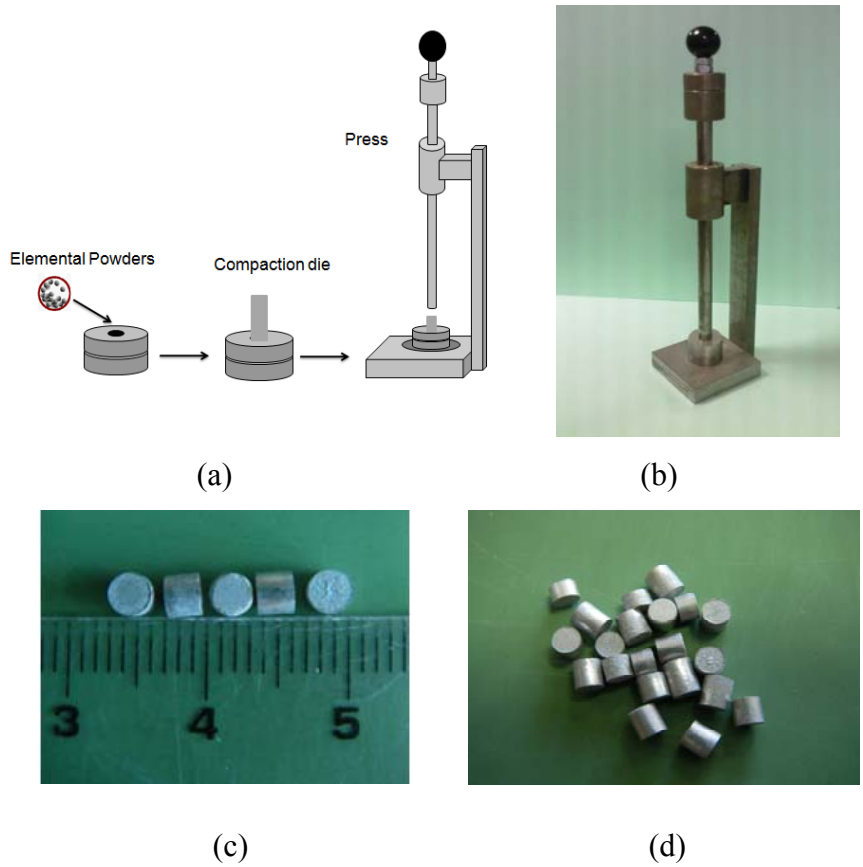

(a) (b)

(c) (d)

Figure 3. 5. Granulation of powders, a) Schematic representation of stages involved in granulation, b) photograph of the press used for granulation, c) and d) cylindrical granules of Mg obtained from -325 mesh powders.

Consolidation (ECAP): Cu blocks with embedded samples were then consolidated via equal channel angular pressing (ECAP), Figure 3.6. Two types of dies have been used for this process. Initial experiments were carried out with a die with 90° channel angle so that the strain (simple shear) imposed on the sample was approximately ε= 1, Segal et al. (1995). A total of four passes were applied, with 90º rotation around longitudinal direction, after each pass. Thus, the sample was deformed to a total true strain of ε=4.

Most experiments, were carried out in parallel ECAP die, Figure 3.7. Here the die incorporates two deformation zones each with a 120° channel angle, Raab et al. (2005). This geometry generates high hydrostatic pressure which by preventing the failure of Cu block, helps consolidation of the embedded sample. In the adopted geometry, one passage of the sample through the die yields a true strain of ε=1.2. An advantage of parallel ECAP is that the process can be automated quite easily, i. e. sample can be repeatedly pushed backward and forward, accumulating extreme strains. Most samples in this work were subjected to 8 passes of ECAP deformation without failure.

Post Annealing: Following ECAP deformation, samples are annealed under Ar atmosphere to assist the formation of intermetallic phases. Where temperature was ≤400 °C, annealing was carried out while the sample was kept in the Cu block. In other cases, the sample was removed from Cu block and annealing was carried out in a tube (vertical) furnace under continuous flow of Ar gas of high purity. Highest annealing temperature employed was 950 °C.

Conditions of post annealing treatment, together with parameters employed in the preceding stages of sample preparation, are given in Table 3.1.

Hydrogenation: Hydrogenation experiments always started with milling of annealed powders for 15-30 minutes in a Spexmill**.** The hydrogen absorption properties of the powders were investigated in a Sievert's type apparatus.

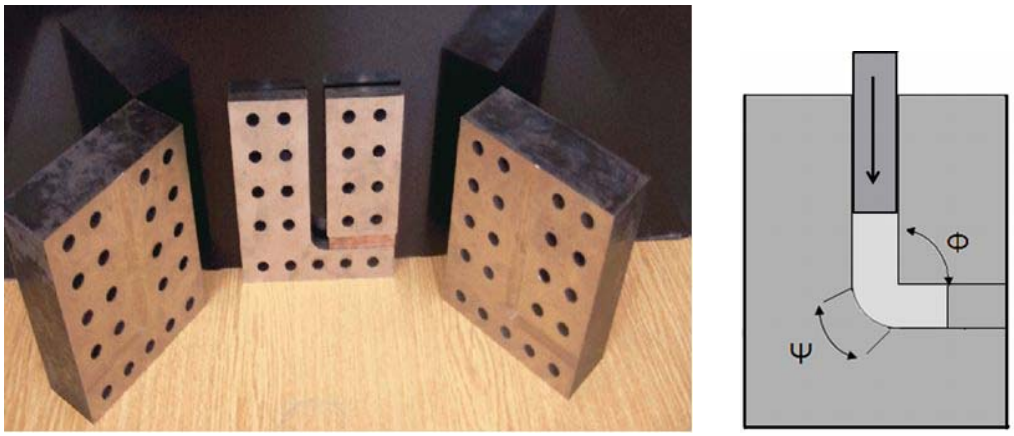

(a) (b)

Figure 3. 6 a) Photograph of die used for ECAP deformation, b) geometry of the die Φ =90°,Ψ= 20°

(a) (b)

Figure 3. 7 a) Photograph of the parallel channel die used for ECAP deformation. Inlay shows a photograph of a sample during passage through the die. b) geometry of the die, Φ = 120^{o}, Ψ= 60°

.

Table 3. 1 Processes and parameters used in the construction of material library

System	Mixing	Consolidation	Annealing Treatment
Mg-Ni	Mg (≤44 μm), Ni (≤44 μm), SPEX milled (15 min.), Ball to powder ratio 20:1	Hot compaction (400 ^{o}C, 6 hrs at a pressure of 400 MPa) Severe plastic deformation (ϕ=90^{o}, 4 passes, total strain ε=4.0)	400° C, 6 hrs
Mg-Ni	Mg (≤44 μm), Ni (≤44 μm)	Compaction in alternating layer form and sintering Compacted (400 MPa), swaged (50 %), sintered (350^{o}C, 6 hrs) Severe plastic deformation (ϕ =120° , 8 passes, total strain ε =9.6)	490° C, 65 hrs
Mg-Ni-Ti	Mg (≤44 μm), Ni (≤44 μm), Ti (≤44 μm) SPEX milled (15 min), Ball to powder ratio 20:1	Hot compaction (375 ^{o}C, 6 hrs at a pressure of 400 MPa) Severe plastic deformation (ϕ=90^{o}, 4 passes, total strain ε=4.0)	400° C, 6 hrs
Mg-Ni-Ti	Mg (≤44 μm), Ni (≤44 μm), Ti (≤44 μm)	Compaction in alternating layer form and sintering Compacted (400 MPa), swaged (50 %), sintered (350^{o}C, 6 hrs) Severe plastic deformation (ϕ =120° , 8 passes, total strain ε =9.6)	490° C, 65 hrs
$MgNi_2$- Ti-Ni (Field A)	$MgNi_2$ (≤44 μm), Ni (≤44 μm) Ti (≤ 44 μm)	Compaction in granule form and sintering Swaging and sintering Swaging (50 %), sintering (12 hrs at 350 °C) Severe plastic deformation (ϕ =120° , 8 passes, total strain ε =9.6)	950°C for 10 hrs

System	Mixing	Consolidation	Annealing Treatment
$MgNi_2$- Ti-Ni (Field A)	$MgNi_2$ (≥44 μm), Ni (≈10 μm), Ti (≤150 μm)	Swaging and sintering Swaging (50 %), Sintering (12 hrs at 350 °C)	850° C, 10 hrs
	SPEX milled (15 min). Ball to powder ratio 20:1	Severe plastic deformation (ϕ=120° die, total strain ε=9.6)Severe	
Mg-Ti-$MgNi_2$ (Field B)	$MgNi_2$ (≤44 μm), Mg (≤44 μm) Ti (≤ 150 μm)	Swaging and sintering Swaging (50 %), sintering (12 hrs at 350 °C)	400° C, 60 hrs
	SPEX milled (15 min). Ball to powder ratio 20:1	Severe plastic deformation (ϕ=120° die, 8 passes, total strain ε=9.6)	

Typically samples were loaded with 5 bar of hydrogen pressure. Pressure-temperature curve were recorded under isochronal heating conditions which involved heating the reactor up to 400-450 ºC with a rate of typically 5 ºC/min. The sorption behavior was followed by monitoring the pressure change as a function of temperature. Similar experiments carried out with Ar were used for comparison.

Characterization: Identification of hydrogen storage phase was carried out by X-ray diffraction(Cu K α). For this purpose XRD patterns were recorded before and after the hydrogenation experiment.

Structural characterization of samples was carried out using SEM. Elemental analysis of local regions as observed in SEM was carried out with EDS. Care was taken to accumulate enough counts before carrying out the local analysis.

CHAPTER 4

RESULTS AND DISCUSSIONS

Results with regard to combinatorial search for hydrogen storage alloys will be given first for Mg-Ni binary and then for Mg-Ni-Ti ternary systems.

4.1 Mg-Ni

Material Library: Two different sample preparation procedures were used for Mg-Ni; powder route and alternating layer approach (see Table 3.1).

In the powder route, Mg-Ni sample in the form of mixed powders was hot compacted, deformed and annealed at 400 ^{o}C. SEM images of the sample after hot compaction are given in Figure 4.1 (a). The structure as recorded in backscattered electron mode comprises three regions of different contrast. XRD pattern of this sample is given in Figure 4.2 (a). The pattern verifies the presence of this three phase structure. These are Ni, Mg_2Ni, and a minor Mg phase. Following ECAP deformation, microstructure ,given in Figure 4.1 (b), seems to have a fragmented appearance. XRD at this stage is little affected, only difference is that the peaks broadened quite significantly as shown in Figure 4.2 (b). Post annealing treatment which aims to develop all phases in the binary system yields essentially the same structure. Only difference is related to Mg_2Ni phase which has increased in its proportion as shown in Figure 4.2 (c).

The results reported above indicate that the powder method is unsuccessful in yielding all phases in the binary system. $MgNi_2$ which appear as an intermetallic in the current system could not be formed in the sample.

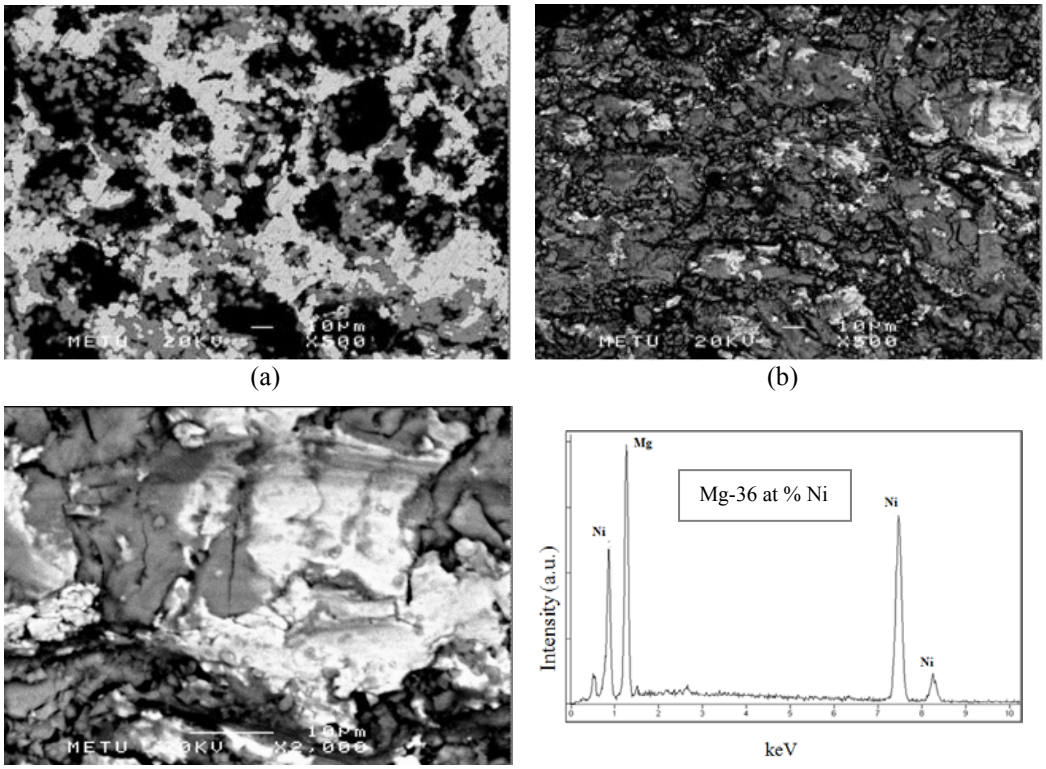

Figure 4. 1 Mg-Ni sample.,a) hot compacted at 400 °C, b) ECAP deformed to ε=4, c) post annealed at 400°C. SEM images are recorded in BSE mode. d) refers to EDS analysis of the gray phase in (c) yields Mg_2Ni.

Noting that the powder approach yielded a partial success, the procedure was modified to employ the layer approach. Alternate layers of metallic powders; Mg and Ni each 2 mm thick were loosely compacted, Table 3.1, and the sample was ECAP deformed to a true strain of ε=9.6, i.e. twice the strain that imposed above. The sample was finally annealed at 490^{o}C. for 65 hrs. A longitudinal section of the final sample is shown in Figure 4.3.

Figure 4.4 (a) shows the microstructure of the post annealed sample. The region shown here is typical and comprises a variety of phases, marked 1-4. The region 1, as verified by EDS analysis was pure Ni as shown in Figure 4.4 (b). Similarly the region 4 is pure Mg. Analysis from regions 2 and 3 yielded a variety of compositions containing both Mg and Ni. Figure 4.5 (a) refers to such a region

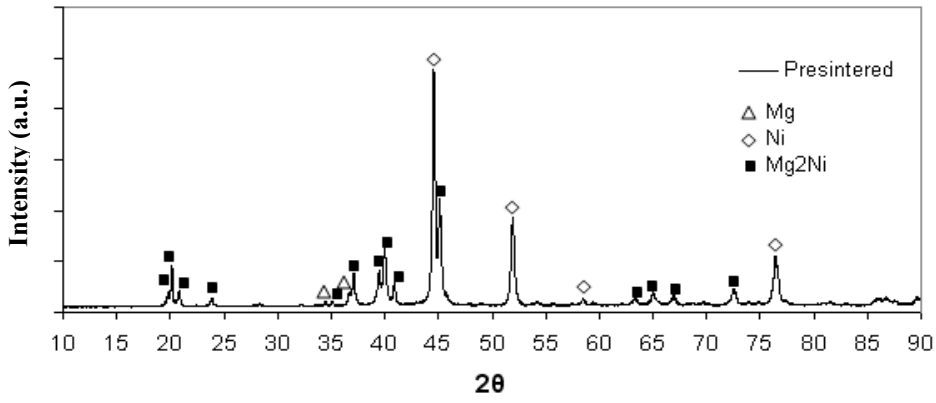

(a)

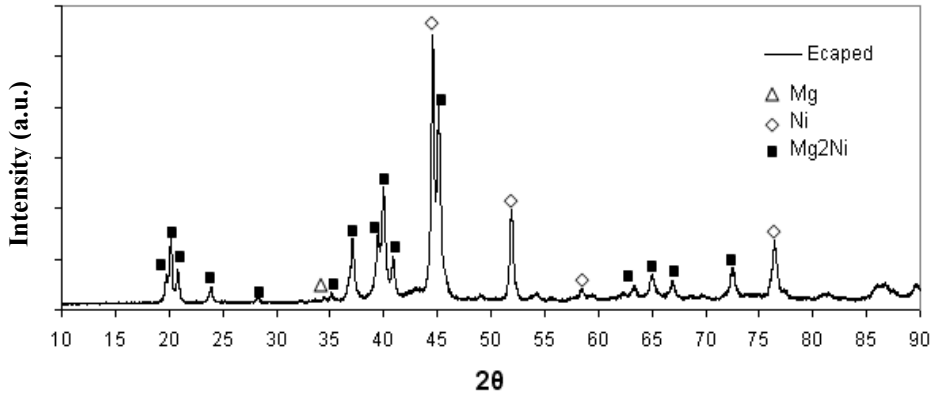

(b)

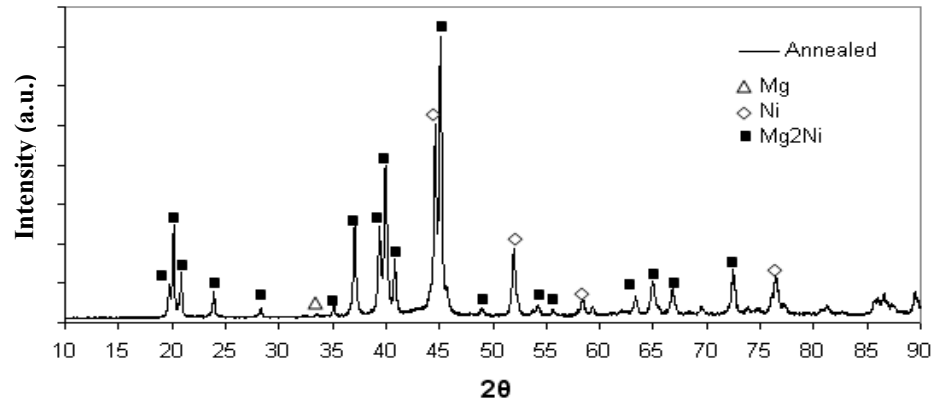

(c)

Figure 4. 2 XRD pattern of Mg-Ni sample, a) as-compacted, b) ECAP deformed, c) post annealed

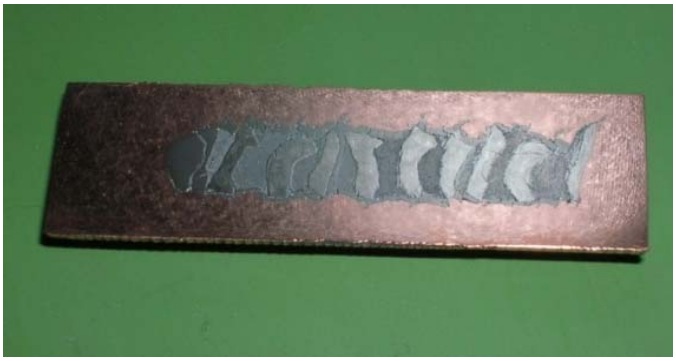

Figure 4. 3 Photograph of longitudinal section of a Cu block with embedded layers of Mg-Ni

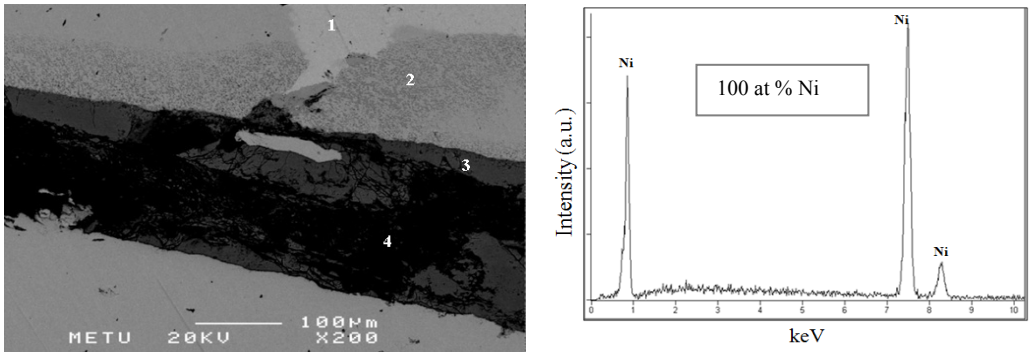

(a) (b)

Figure 4. 4 Mg-Ni sample annealed at 490 °C . a) SEM image, b) EDS analysis of region 1

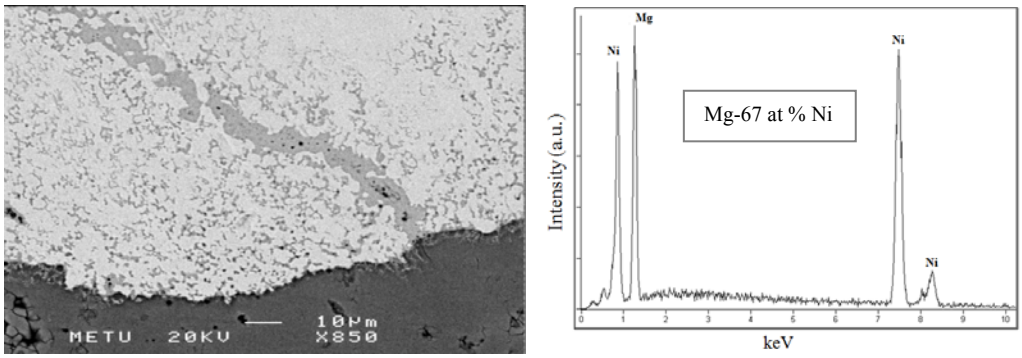

(a) (b)

Figure 4. 5 a)SEM image of Mg-Ni sample (annealed at 490 °C) at higher magnification, b) EDS analysis of gray region running diagonally in bright region, i.e. $MgNi_2$

at a higher magnification. Here the relatively dark regions running diagonally in the structure yields an analysis with a composition of $MgNi_2$, Figure 4.5 (b). Thus it appears that region 2 and 3 are made up of phases of Mg_2Ni and $MgNi_2$.

XRD pattern for this sample is given in Figure 4.6. Here the pattern comprises of Mg, Ni, and the intermetallics Mg_2Ni and $MgNi_2$. Thus, the identified phases verify the above observations, though the $MgNi_2$ phase does not yield well defined peaks of its own, since it mixes with peaks of others. Although the use of alternating layers together with a heavy strain imposed via ECAP was successful in yielding all phases in Mg-Ni binary, the intermetallics formed were small in their proportions. This is the direct outcome of the coarseness of the structure where the interface boundaries are necessarily less common.

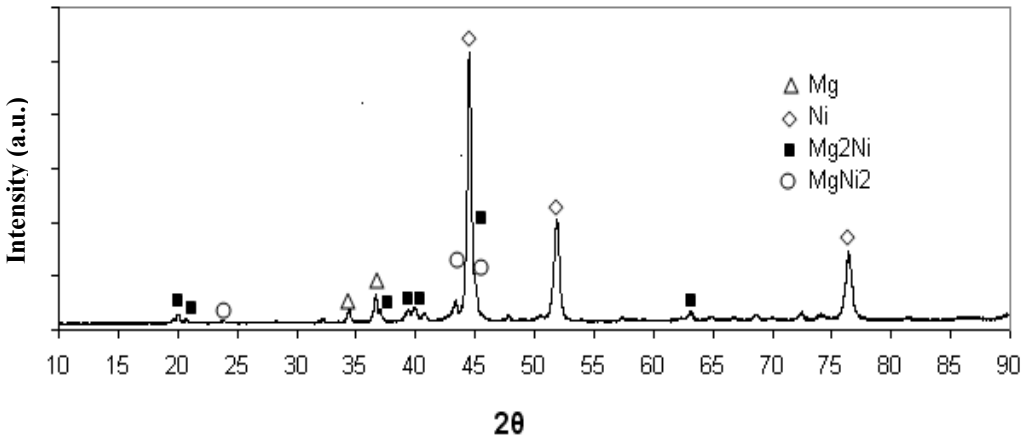

Figure 4. 6 XRD pattern of Mg-Ni sample produced from alternating layers, annealed at 490 °C.

Screening: Screening of the Mg-Ni sample for hydrogen storage compositions involved hydrogenation of the sample followed by its examination with X-ray diffraction. Hydrogenation behavior of the Mg-Ni sample after post annealing is given in Figure 4.7. This refers to a pressure change under a constant volume as the sample was heated under hydrogen atmosphere of initially 5 bar pressure. In the sample, as compared to that recorded with Ar, there seems to be a lack of

pressure rise at temperatures around 75°C. This turns into a clear pressure drop, starting from 160 ºC which continues up to 325°C indicating that there is/are phase(s), in the sample, that absorb hydrogen. Then on, the pressure picks up presumably, due to the release of absorbed hydrogen, and reaches nearly to the same level as that of Ar at temperatures near 400 °C.

To determine which phases absorb hydrogen, several absorption/desorption cycles were applied to the sample (total desorption has been carried out under dynamic vacuum at 400 °C). Finally, the sample was cooled from 300 ºC under hydrogen pressure, down to room temperature and examined with X-ray diffraction. XRD pattern shown in Figure 8 comprises Mg_2NiH4 ,Mg and Ni . When this XRD is compared with the previous pattern, Figure 4.2 (c), it is clear that it is Mg_2Ni phase is affected by hydrogenation. Thus Mg_2Ni hydrogenates to Mg_2NiH_4 which according to its reflections have cubic structure.

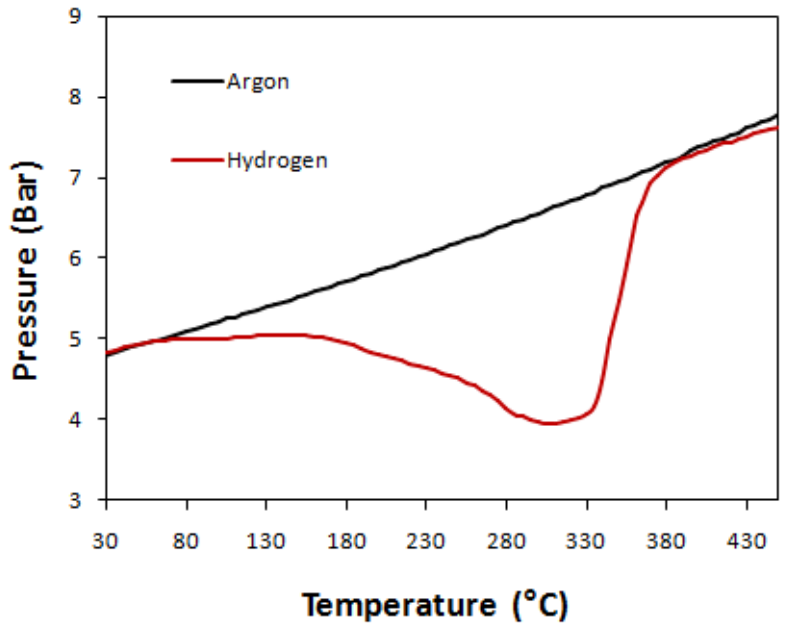

Figure 4. 7 Pressure-temperature curve for Mg-Ni recorded in a constant volume under hydrogen pressure of approx. 5 bar. Linear variation recorded with Ar is also shown.

It should be noted that XRD pattern given after hydrogenation, Figure 4.8, contains some additional peaks. These peaks implies the formation of a new phase. This is $MgNi_2$. This shows that hydriding/dehydriding cycle assisted the formation of $MgNi_2$. The formation of this phase might be due to extended exposure of the sample to 400-440 °C where Mg_2Ni reacting with Ni could lead to formation of $MgNi_2$ Song (1999), or it could be due to the partial transformation of Mg_2Ni to $MgNi_2$ due to some evaporation of Mg, Hatano et al. (2002).

For the current system, the phases expected are Mg, Mg_2Ni, $MgNi_2$ and Ni. Of these, Mg_2Ni and Ni phases were dominant in the annealed sample. Although Mg was present in the structure, it was not a distinct phase in the XRD pattern. This is probably due to the consumption of a greater portion of Mg in the internal reaction yielding Mg_2Ni phase. $MgNi_2$ phase was difficult to form in the annealing treatment, though it could form as a result of several hydrogenation and dehydrogenation cycles.

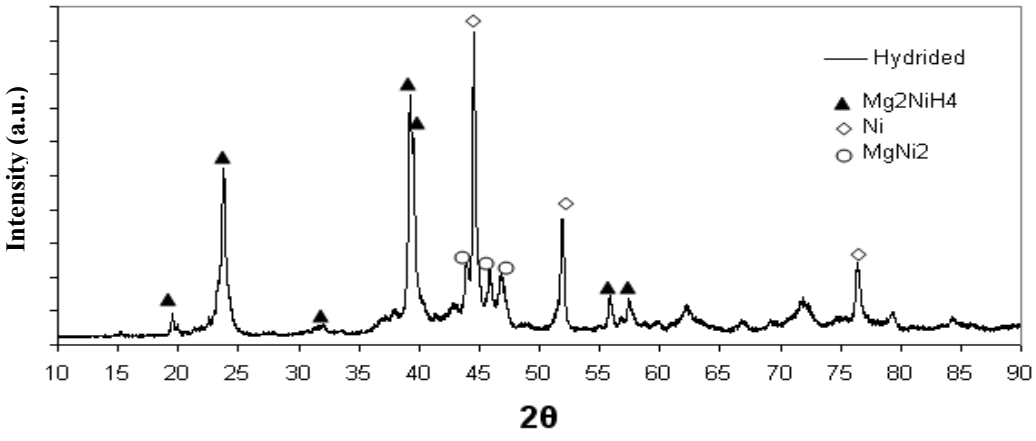

Figure 4. 8 XRD pattern of Mg-Ni, after hydrogenation, i.e. Mg-Ni under a hydrogen pressure of 5 bar heated up to 300 °C and cooled to room temperature. Note the formation of Mg_2NiH_4 and $MgNi_2$.

In conclusion, combinatorial search procedures used for Mg-Ni system successfully yielded all relevant phases, and have shown that Mg_2Ni is a reactive phase which can be employed as hydrogen storage alloy. As far as the procedure is concerned the current system has two drawbacks; one is that $MgNi_2$ phase could not be formed at the expected stage, and second Mg which is known to absorb hydrogen could not be identified with the procedure as implemented in the current sample.

4.2 Mg-Ni-Ti

Material Library: Mg-Ni-Ti system was investigated by similar procedures, employing both powder and alternating layer approaches. Here, first the ternary Mg-Ni-Ti as a whole will be evaluated, then the procedures will be applied to two sub systems; $MgNi_2$-Ni-Ti and $MgNi_2$-Mg-Ti.

The powder approach as described above (Mg, Ni, Ti powders, hot compacted and deformed, see Table 3.1, was annealed at 400 ^oC) yielded essentially the same result as in the binary. In addition to starting phases; Mg, Ni, Ti, only other phase which was present was Mg_2Ni. Microstructures and XRD patterns of the sample at various stages of processing are given in Figures 4.9 and 4.10, respectively. As seen in Figure 4.10 (c), Mg_2Ni peaks, unlike the case in Mg-Ni binary is very weak, implying that the intermetallic formed is quite small in proportion. This could be attributed to the presence of the third element Ti in the structure that minimizes Mg-Ni contact.

Apart from Mg_2Ni, no other binary or ternary intermetallics were detected in the structure. This indicates that a sintering temperature of 400 °C is probably not enough for the formation of most phases in the ternary system.

In the alternating layer approach, the samples (loosely compacted, metallic powders; Mg and Ni surrounded by Ti in a Cu rod, ECAP deformed to ε=9.6) was annealed for 65 hrs at a higher temperature of 490 °C. A typical

microstructure in this sample is given in Figure 4.11 (a). Here regions of different contrast are marked 1-5. Regions 1, 4 and 5 as verified by the EDS analysis are Ni, Ti and Mg, respectively. Regions inbetween Ni and Mg yield Mg_2Ni. Regions 2 and 3 involve mixture of phases. Here region 3 is of particular interest which involves elements Ti and Ni. A magnified image of region 3 taken BSE mode ,Figure 4.12 (a), shows the presence of three phases as judged from the differences in their contrasts. The dark phase is Ti. A region surrounding this phase, which appear gray, clearly visible on lower left region, has a composition of Ti_2Ni ,Figure 4.12 (b). Outer regions, which appear bright, has a composition that nearly matches TiNi ,Figure 4.12 (c). $TiNi_3$ phase was not detected in the microstrucrure. XRD pattern taken from the sample is dominated by pure elements. The other peaks were extremely weak emerging from the background level hindering peak identification.

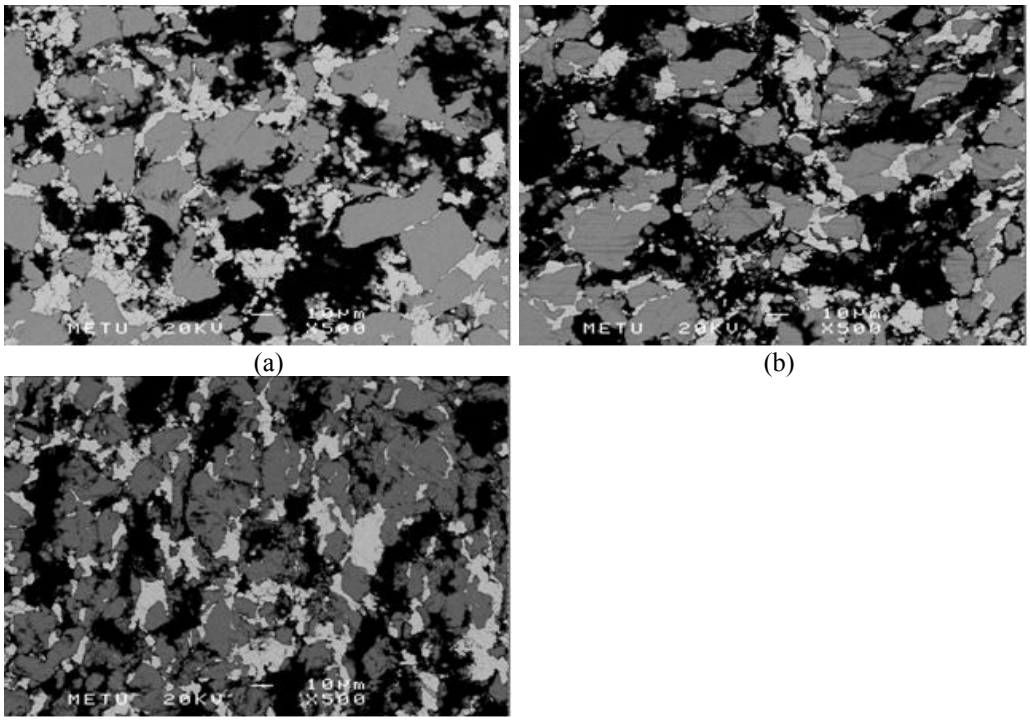

(a) (b)

(c)

Figure 4. 9 SEM images of Mg-Ni-Ti sample , a) as-compacted, b) ECAP deformed, c) post annealed at 400 °C.

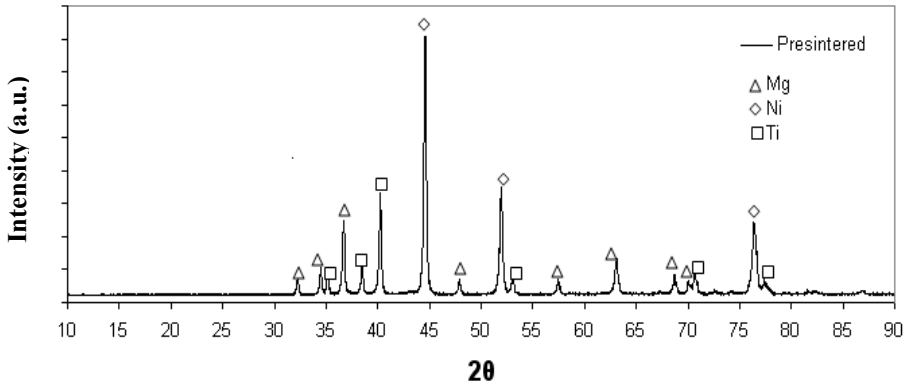

(a)

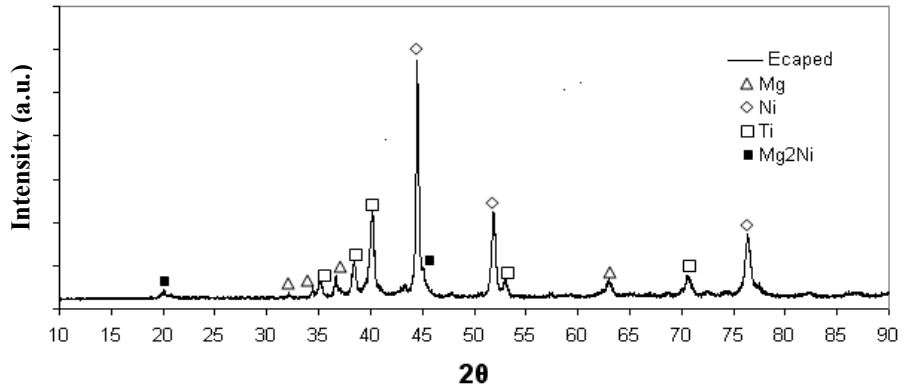

(b)

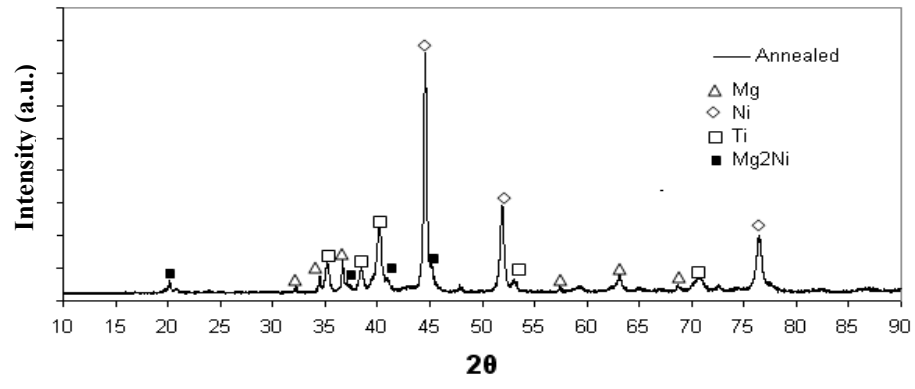

(c)

Figure 4. 10 XRD pattern of Mg-Ni-Ti, a) as-compacted, b) ECAP deformed, c) post annealed at 400 ^{o}C.

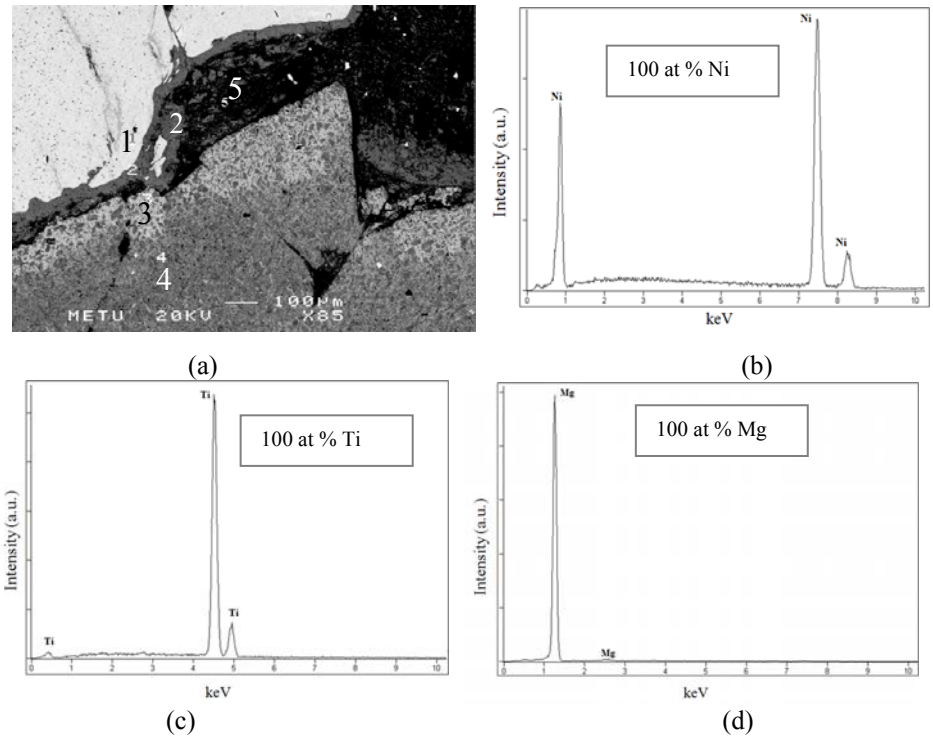

Figure 4. 11 Mg-Ni-Ti sample produced via alternating layer approach. a) SEM image of phases formed in post annealing treatment, b), c) and d) refers to EDS analysis of region 1,4 and 5 respectively

Observations reported above show that both mixed powder and alternating layer approaches were not successful in yielding all the expected phases. The intermetallic phases that formed, in alternating layer approach, were small in proportions, and were not noteworthy in the XRD.

To enhance the intermetallic formation, samples were prepared with length scales finer than that of alternating layer approach. For this aim, starting powders were granulated to a size of 2-3 mm. In addition to the adjustment in the length scale, it would be desirable to select as high an annealing temperatures as possible. It appears that the annealing temperatures selected so far were too low for some of the phases whose melting temperature are in excess of 1000 °C, e.g. 1310 °C for TiNi, 1380 °C for $TiNi_3$. Since Mg has a quite low

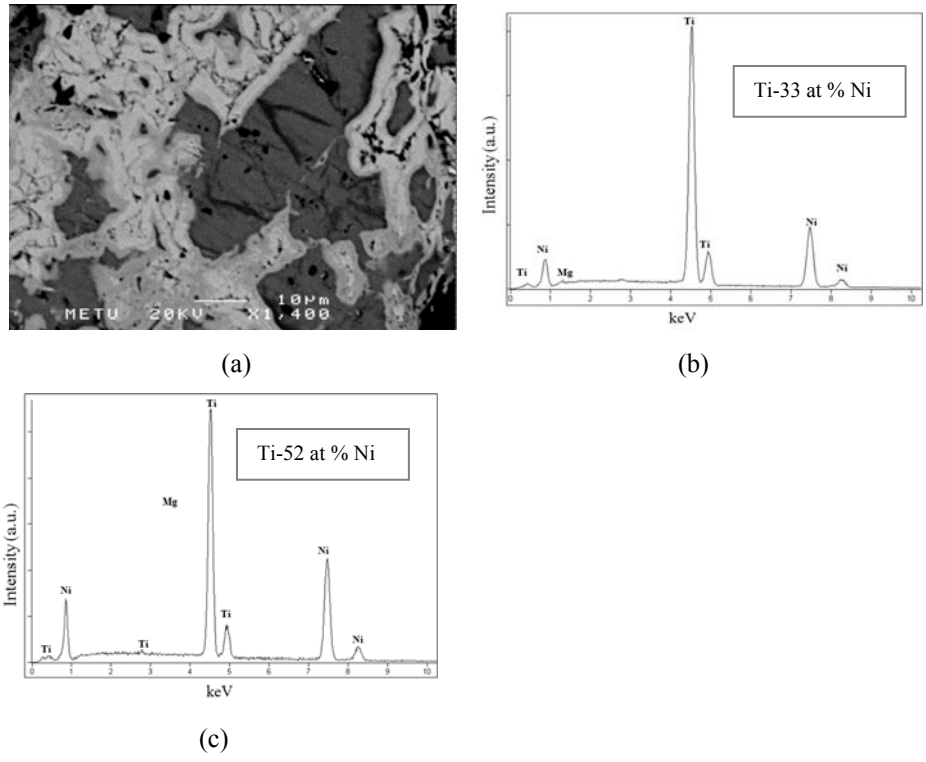

Figure 4. 12 . a) SEM image of a region (region 3 in Figure 4.11) in Mg-Ni-Ti alternating layer sample. (b) and (c) refer to EDS spectra recorded from gray and white regions.

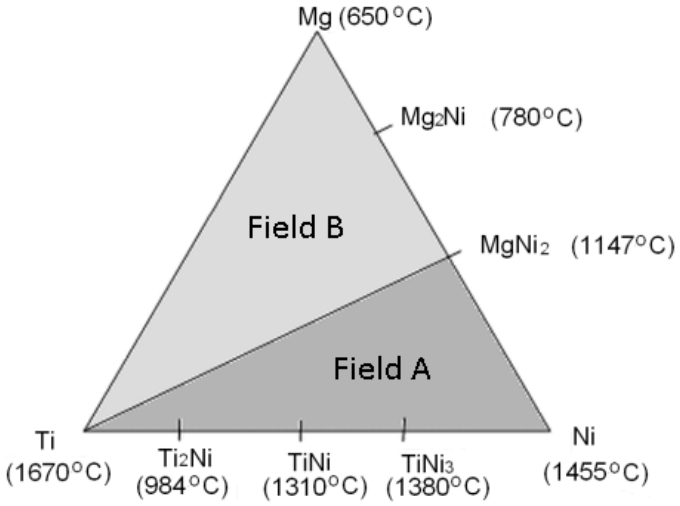

Figure 4. 13 Partitioning of Mg-Ti-Ni ternary phase diagram. Field A comprises phases of high melting or solidus temperature, Field B is expected to comprise those with low melting points.

melting point (650 °C) the use of single sample to form all the relevant phases without exceeding their melting or solidus temperature is not realistic. Thus to enhance the intermetallic formation, two samples maybe used for the current system. This is the ternary system ,Figure 4.13, can be split into two subfields; $MgNi_2$-Ni-Ti, Mg-Ti-$MgNi_2$ referred to Field A and Field B, respectively. The former is expected to involve phases of high melting point where the latter involves low melting point phases like Mg.

The sample for Field A was prepared using granules of $MgNi_2$, Ni, Ti. The granules were compacted in the Cu rod by swaging followed by ECAP deformation to a ε=9.6 and post annealed at 950°C for 10 hrs, Table 3.1. Macrostructure resulting from this treatment is given in the SEM image in Figure 4.14. Regions of different contrast in this structure are approximately 3 mm in size, reflecting the length scale of the original structure. Here, regions marked 1-3 are Ti, Ni, $MgNi_2$, respectively. The boundary between Ti -Ni (regions 1 and 2 in the figure) is reproduced in Figure 4.15 (a) at a higher magnification. Compositions in this region correspond to TiNi intermetallic.

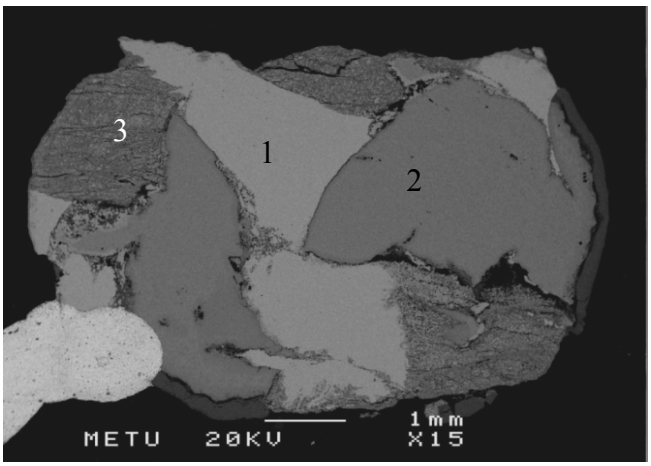

Figure 4. 14 $MgNi_2$-Ti-Ni sample produced from granules of 2-3 mm in size. Regions of different contrasts are $MgNi_2$, Ti, Ni. Region 1 is Ni, region 2 is Ti and 3 is $MgNi_2$

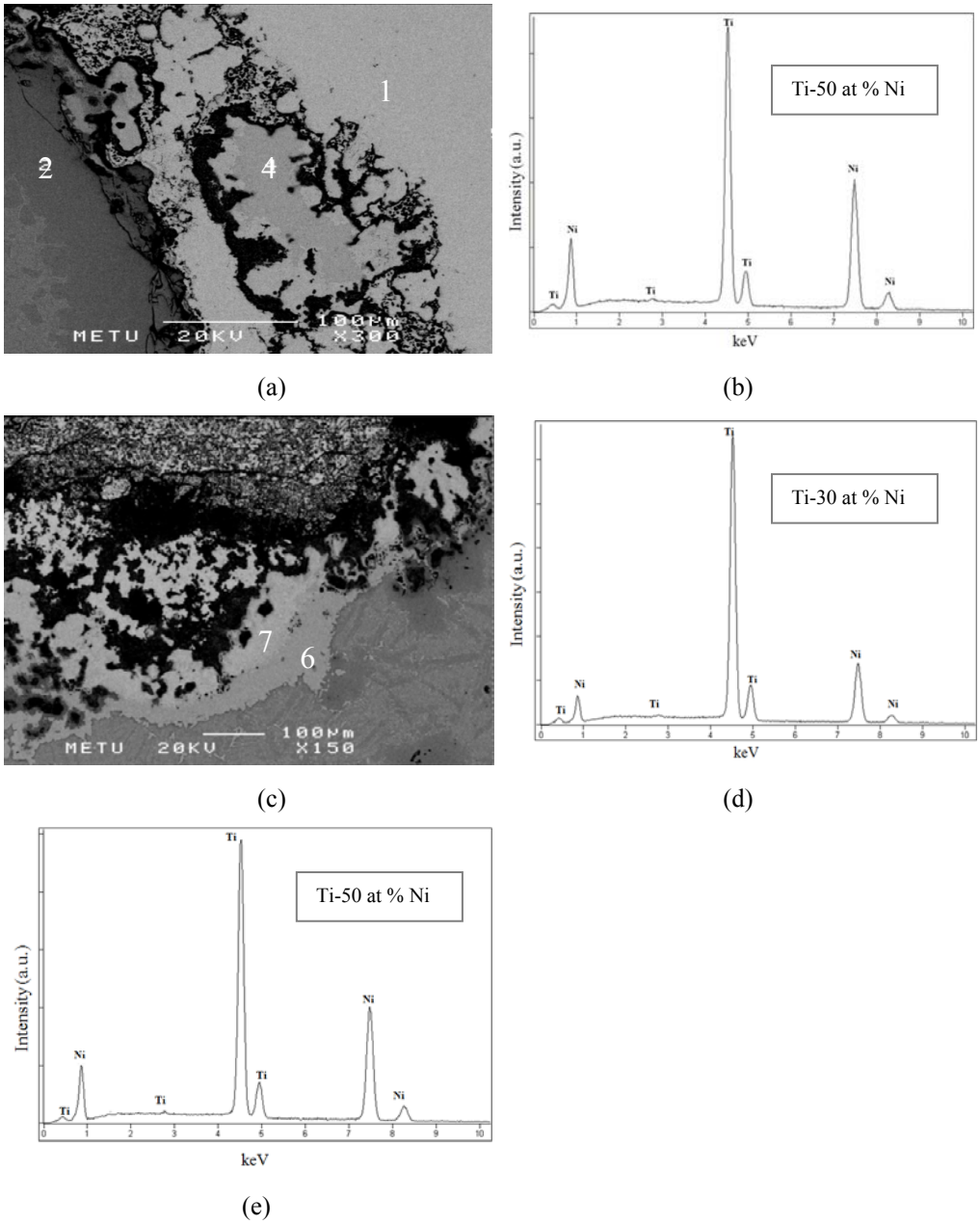

Figure 4. 15 SEM images and EDS analysis $MgNi_2$-Ti-Ni. a) SEM images of Ti-Ni phase boundary. Region 2 is Ti, region 1 is Ni. b) EDS analysis of region 4, c) SEM image of $MgNi_2$-Ti boundary. d) EDS analysis of region 6, e) EDS analysis of region 7

Similarly, Figure 4.15 (c) shows $MgNi_2$-Ti boundary. The phases observed in this region are TiNi and Ti_2Ni. Surprisingly no Mg bearing compound other than the starting $MgNi_2$ was observed in this region. It appears that Ni in TiNi and Ti_2Ni originates from "$MgNi_2$" phase which had an excess Ni phase in it, see section 3.1.

Considering the binary systems, the Field A should cover such phases; TiNi , Ti_2Ni, $TiNi_3$, and $MgNi_2$. Of these in the current sample TiNi, Ti_2Ni, $MgNi_2$ were observed. $TiNi_3$ phase; however, did not form in the sample. Thus, the method is not fully succsessful in yielding all the phases.

In order to maximize interface area where the reaction occurs, the alternating layer approach was abandoned in favor of powder approach. Thus for Field A, $MgNi_2$, Ni and Ti powders were mixed, compacted and ECAP deformed to a ε=9.6, see Table 3.1 Following ECAP deformation, the sample was post annealed at 850 °C under Ar flow for 10 hrs.

SEM image of this sample is given in Figure 4.16. As seen in the micrograph there are 6 regions of different contrast whose EDS analysis are given in Table 4.1.The region 1 is a two-phase region, with a lamellar arrangement Figure 4.17 (a). EDS analysis of this region yields a composition of 94 at % Ti and 6 at % Ni as shown in Table 4.1. This complies with the expected eutectoid mixture of Ti and Ti_2Ni in the ratio of 81 wt % Ti / 19 wt % Ti_2Ni.

Region 2 neighboring the above region has a composition of 69 at % Ti, 31 at % Ni. This is not far off the intermetallic Ti_2Ni. The region enveloping Ti_2Ni intermetallic marked 3, Figure 4.17 (b), has a composition of 51 at % Ti, 49 at % Ni which is consistent with TiNi intermetallic, Figure 4.17 (c). The following two regions have similar contrast; the region 4, Figure 4.17 (d), has a composition of 26 at % Ti and 74 at % Ni which complies with the intermetallic iNi_3 and region 5 is Ni, Figure 4.17 (e).Region 6 has a composition close to $MgNi_2$ that seems to originate from the starting powder.

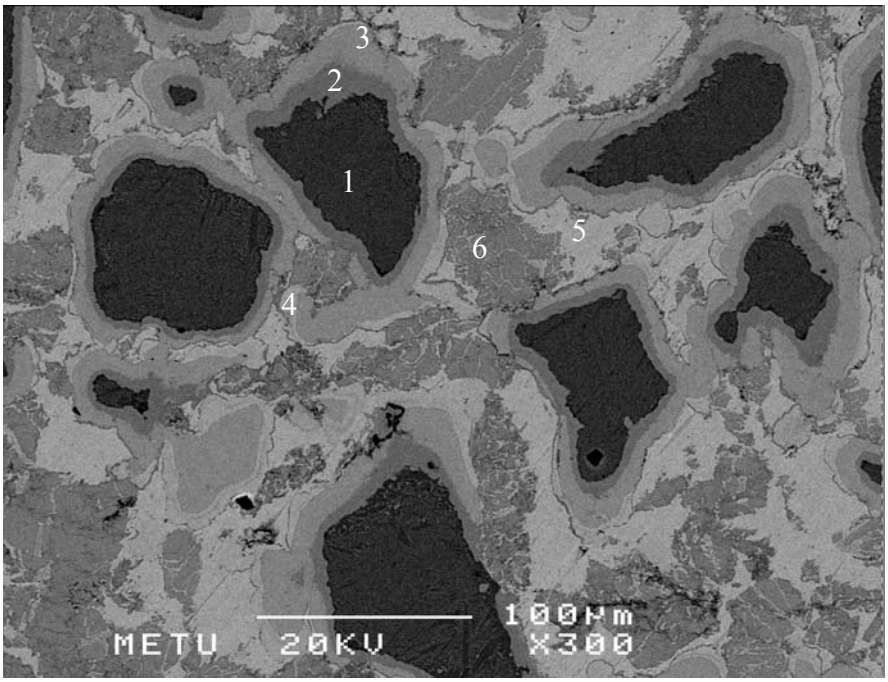

Figure 4. 16 SEM image of $MgNi_2$-Ti-Ni sample annealed at 850 °C. Regions of different contrasts are numbered 1-6..

Table 4. 1Elemental analysis of localities in $MgNi_2$-Ti-Ni sample annealed at 850 °C. Numbers refer to regions in Figure 4.16

Location	Analysis
Region 1	94 at % Ti, 6 at % Ni
Region 2	69 at % Ti, 31 at % Ni
Region 3	51 at % Ti, 49 at % Ni
Region 4	26 at % Ti, 74 at % Ni
Region 5	100 at % Ni
Region 6	72 at % Ni ,28 at % Mg

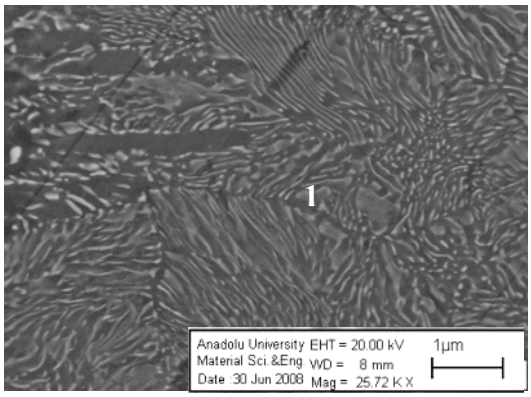
1
Anadolu University EHT = 20.00 kV
Material Sci.&Eng. WD = 8 mm
Date :30 Jun 2008 Mag = 25.72 K X
1µm

(a)

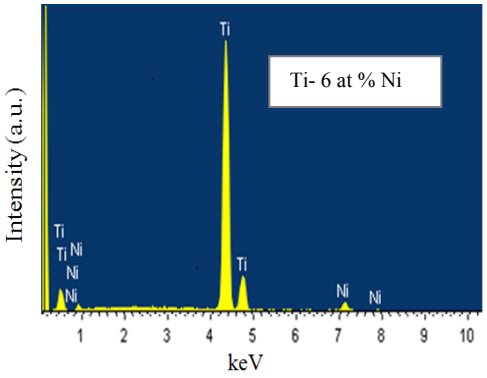
Ti- 6 at % Ni
Intensity (a.u.)
keV
Ti
Ni

(b)

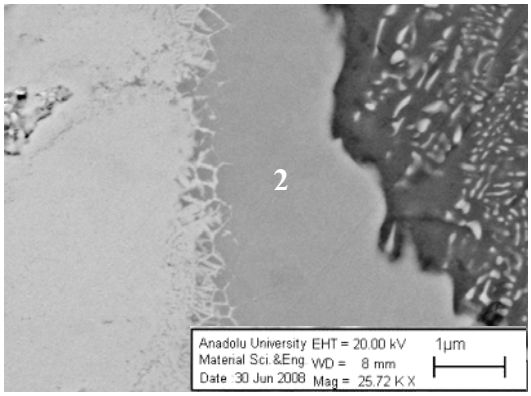
2
Anadolu University EHT = 20.00 kV
Material Sci.&Eng. WD = 8 mm
Date :30 Jun 2008 Mag = 25.72 K X
1µm

(c)

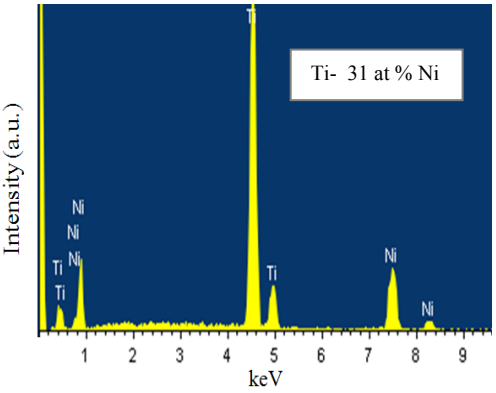
Ti- 31 at % Ni
Intensity (a.u.)
keV
Ti
Ni

(d)

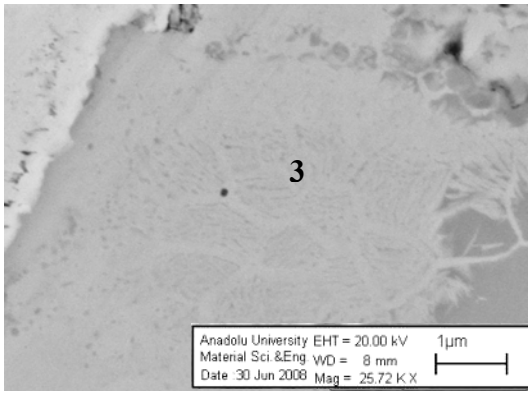
3
Anadolu University EHT = 20.00 kV
Material Sci.&Eng. WD = 8 mm
Date :30 Jun 2008 Mag = 25.72 K X
1µm

(e)

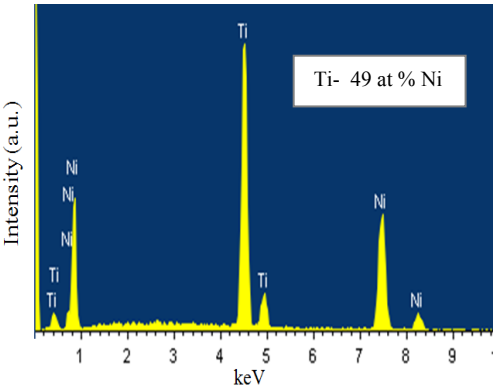
Ti- 49 at % Ni
Intensity (a.u.)
keV
Ti
Ni

(f)

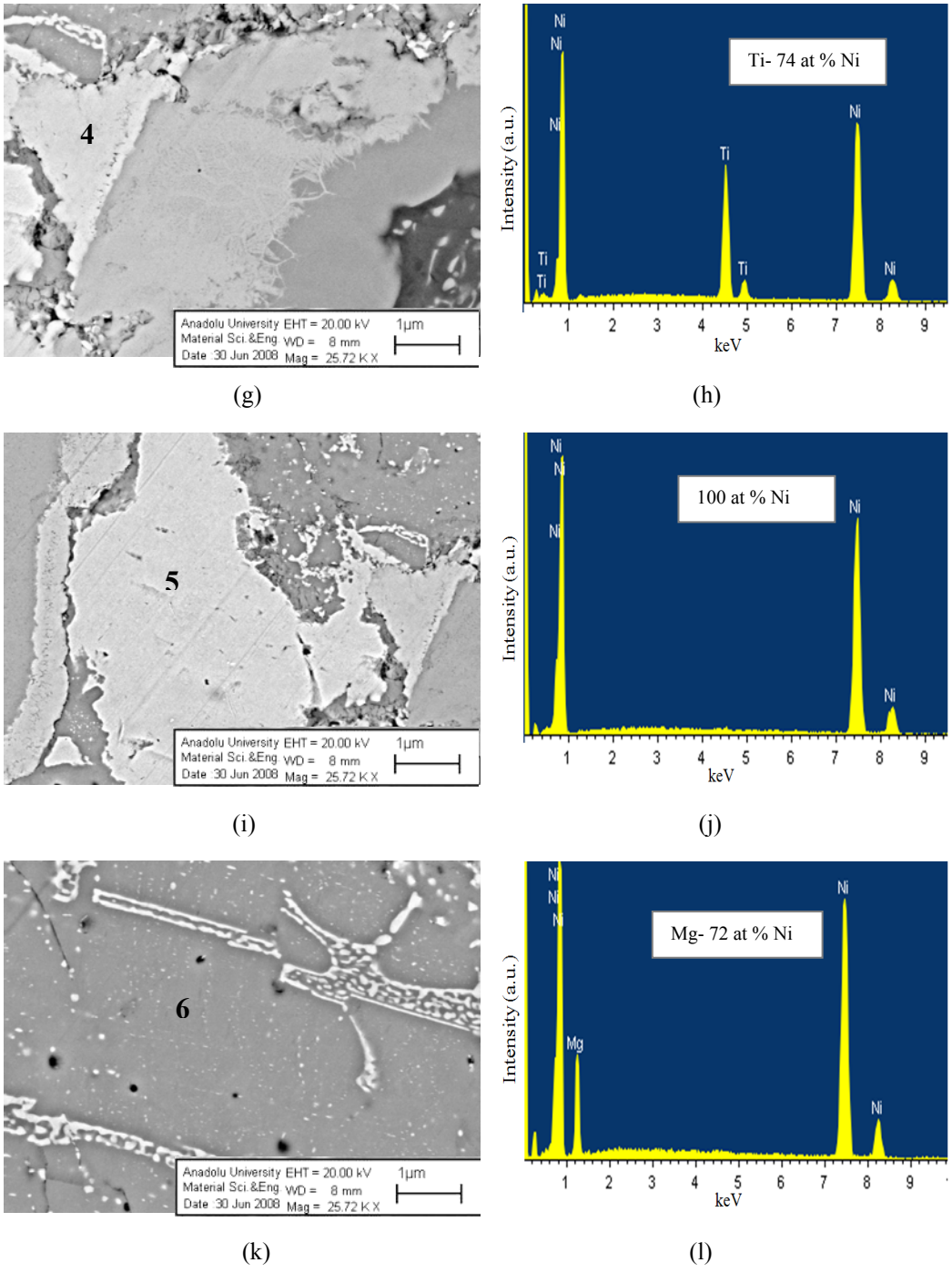

Figure 4. 17 SEM images and EDS analysis refers to region marked in Figure 4.16, $MgNi_2$-Ni-Ti, sample annealed at 850 °C, a) region 1, combining eutectoid mixture of phases Ti and Ti_2Ni, b) EDS analysis of region 1, c) region 2 , d) EDS analysis of region 2, Ti_2Ni, e) region 3, f) EDS analysis of TiNi intermetallic g) region 4, $TiNi_3$ intermetallic, h) EDS analysis of region 4, i) region 5 is Ni, j) EDS analysis of region 5, k) region 6, $MgNi_2$, l) EDS analysis of region6.

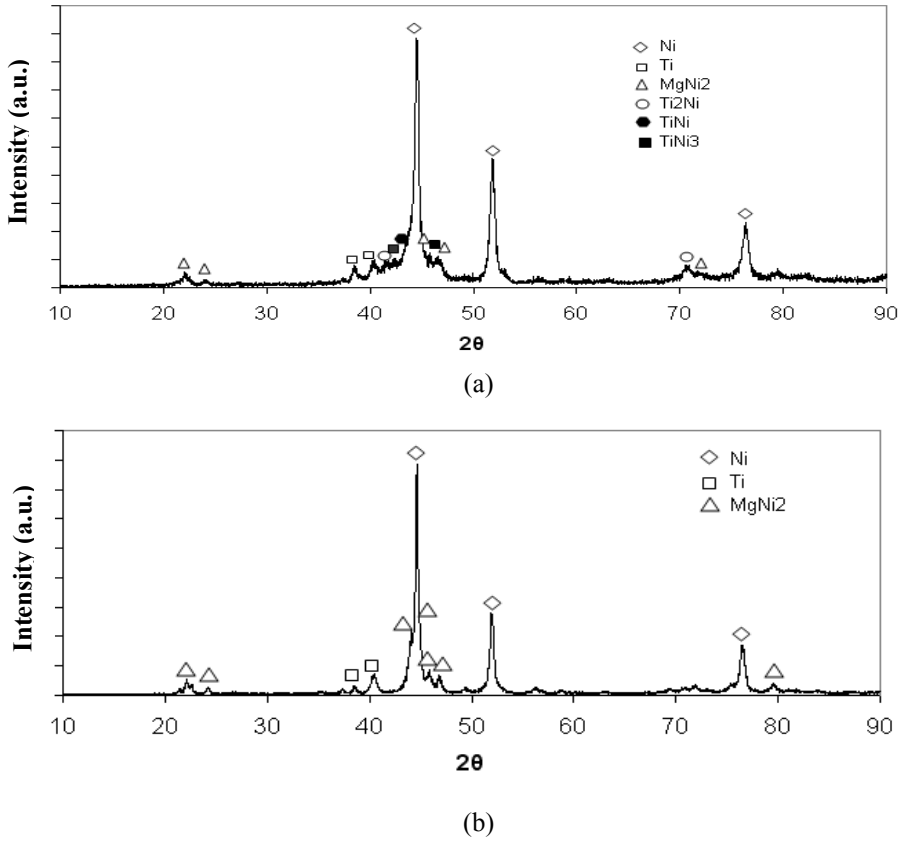

Figure 4. 18 XRD pattern of $MgNi_2$-Ni-Ti sample, a) annealed at 850 °C after ECAP. b) ECAP deformed.

XRD pattern of the annealed sample is given in Figure 4.18 (a).The pattern verifies the starting constituents $MgNi_2$, Ti, Ni. TiNi,Ti_2Ni and $TiNi_3$ are probably present but their peaks are not as distinct, since they overlap with the existing peaks. XRD pattern of the ECAP deformed sample is given Figure 4.18 (b), which verifies $MgNi_2$, Ti and Ni phases.

For Field B, Mg-Ti-$MgNi_2$, the sample was synthesized with the using $MgNi_2$, Ti and Mg powders compacted and ECAP deformed to ε=9.6, see Table 3.1.Following ECAP deformation, the sample was annealed at 400°C for 60 hrs.

Three regions of different contrast, marked 1-3 were observed in the annealed sample , Figure 4.19 (a). SEM image of this region at a higher magnification is

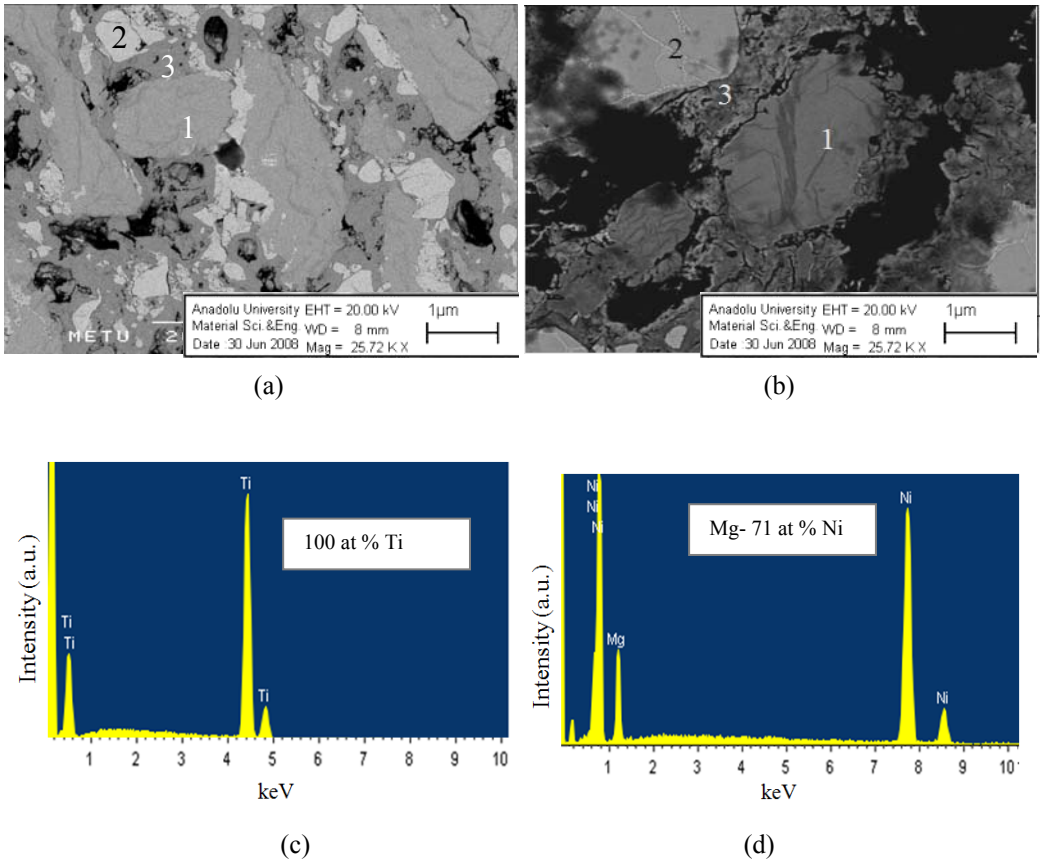

Figure 4. 19 a) SEM image of Mg-Ti-$MgNi_2$sample annealed at 400 °C, and b) at higher magnification, EDS analysis of c) region 1, d) region 2.

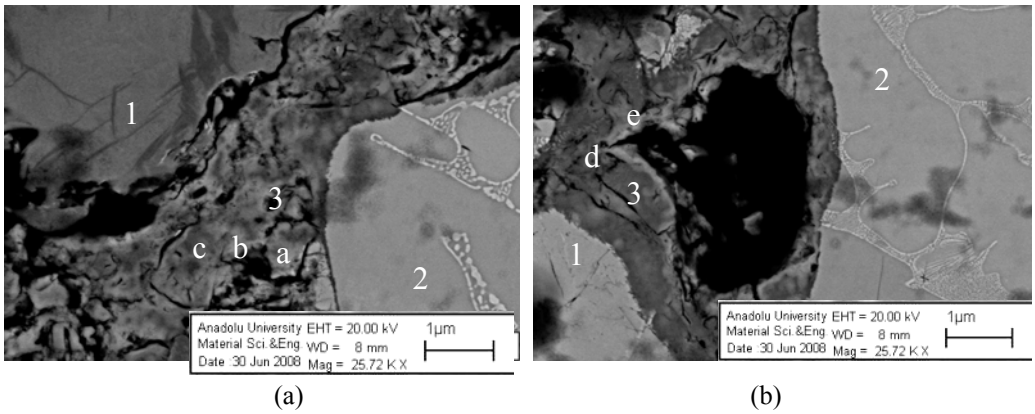

Figure 4. 20 SEM images of regions of Mg-Ti-$MgNi_2$sample annealed at 400 °C, (a) and (b).

given in Figure 4.19 (b). The EDS spectra recorded from these localities are given in Figure 4.19 (c) and (d). As verified by EDS, the region 1 is Ti and the region 2 has a composition of 71 at % Ni and 29 at % Mg. This is a Ni rich region possibly made up of phases; $MgNi_2$ and Ni. The region 3 is reproduced in Figure 4.20 at higher magnification. EDS analysis taken from various locations in this region marked by a-e are given in Table 4.2. As seen in the table some compositions are Ni rich, some nearly equal in their Ni and Mg content. This implies that the location was probably occupied by Mg originally, but consumed as a result of internal reaction of Mg with $MgNi_2$ or Ni.

Table 4. 2 EDS analysis of localities in $MgNi_2$-Ti-Mg sample annealed at 400 °C

Location	Analysis
Region 1	93. 6 at % Ti,6. 4 at % Ni
Region 2	71 at % Ni and 29 at % Mg
Region a	45at%Mg and 55 at% Ni
Region b	30at%Mg and 70at%Ni
Region c	18at%Mg and 82at%Ni
Region d	51at%Mg and 49at%Ni
Region e	37at%Mg and 63at%Ni

XRD pattern of the annealed sample is given in Figure 4.21 (a).The sample comprises Mg_2Ni, $MgNi_2$, Ni. A weak Mg protrusion at the base of $MgNi_2$ peak at $2\theta = 37.16$, (110), can also be identified. Comparison of this pattern with that before annealing, Figure 4.21 (b), reveals that only Mg_2Ni phase has formed as a result of annealing.

There are two routes for the formation of Mg_2Ni. One is the reaction of Mg with Ni which was present as a minor additional phase in the starting $MgNi_2$ powder. The other is the reaction of $MgNi_2$ with Mg.

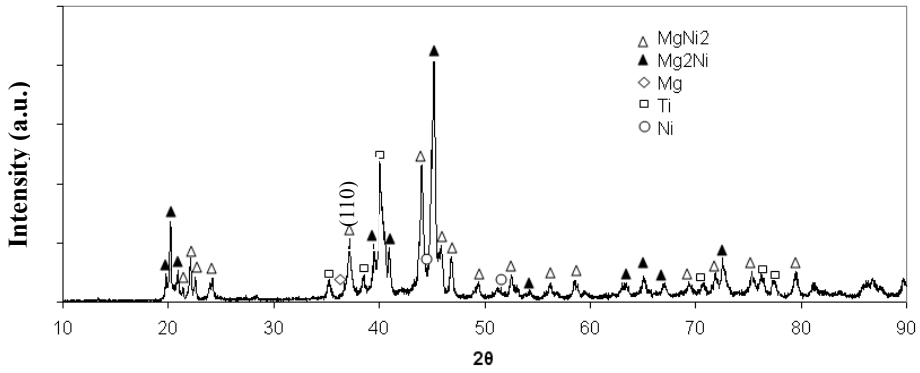

(a)

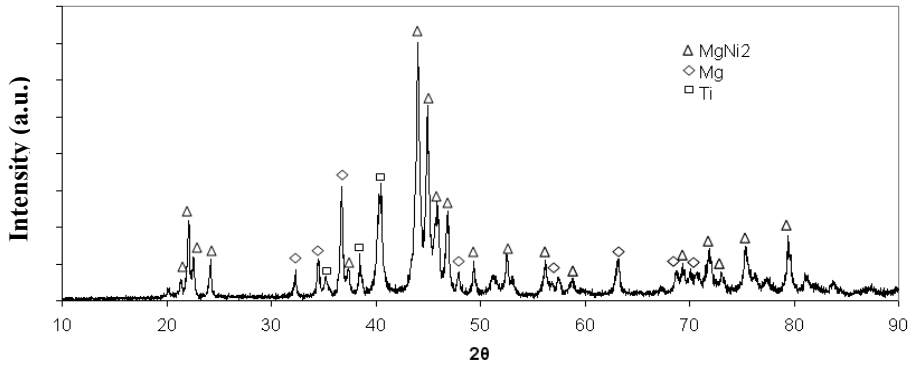

(b)

Figure 4. 21 XRD pattern of a), annealed $MgNi_2$-Mg-Ti, b) ECAP deformed sample

Screening: The annealed $MgNi_2$-Ni-Ti (prepared by powder route) multiphase sample was hydrogenated in the Sievert apparatus for screening. For this purpose, the sample was Spex milled for 15 minutes. The sample loaded with hydrogen of 8 bar pressure in a constant volume and was heated up to 400 °C at a rate of 5 deg/min. Pressure change recorded as a function of temperature is given in Figure 4.22. It is seen that the pressure deviates from linearity at around 100 °C indicating absorption. Following the pressure drop the line runs parallel to that of Ar implying no pressure pick up i.e. no desorption of absorbed hydrogen up to 400 °C.

XRD pattern of the sample removed from the apparatus in hydrogenated condition (cooled under hydrogen pressure) is given Figure 4.23 (a).

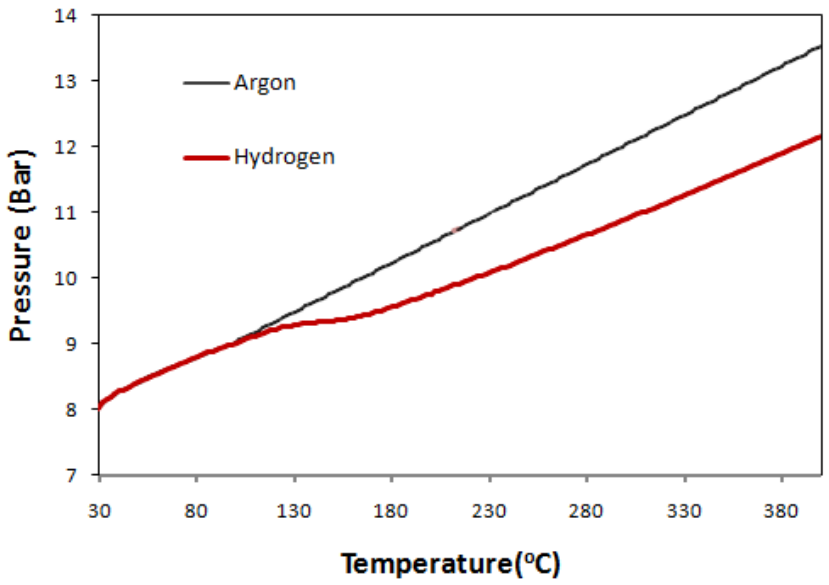

Figure 4. 22 Pressure-temperature curve for $MgNi_2$-Ni-Ti recorded in a constant volume under hydrogen pressure of approx. 8 bar. Linear variation recorded with Ar is also shown.

Examination of this pattern in comparison with that of annealed sample, Figure 4.23 (a), showed that $MgNi_2$, $TiNi_3$ and Ni phases remain unaffected by hydrogenation. Formation of a new phase, TiH_2, was observed. TiNiH and Ti_2NiH may also be present but their presence cannot be ascertained clearly due to weak intensities.

In order to identify the hydrogen sorbing phase more clearly, following several cycles of hydrogenation and dehydrogenation, a sample was removed from the apparatus in the dehydrogenated form, i.e. the sample was cooled from 300 °C under vacuum. XRD pattern of the dehydrogenated sample is given in Figure 4.23 (b). It should be noted that TiH_2 is still present in the sample. TiNiH and Ti_2NiH whose peaks were possibly present in the hydrogenated sample have returned to TiNi and Ti_2Ni upon dehydrogenation. The expanded portion of the XRD patterns in interval of $38°<2\theta<45°$ for hydrogenated and dehydrogenated samples are superimposed in Figure 24.

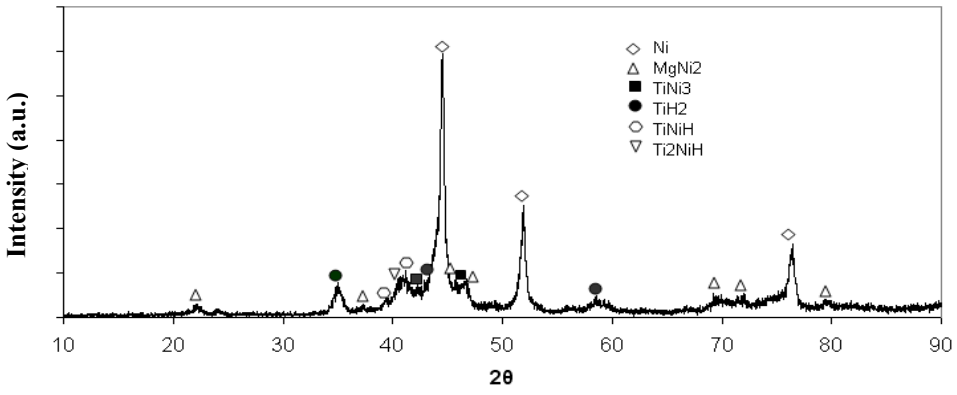

(a)

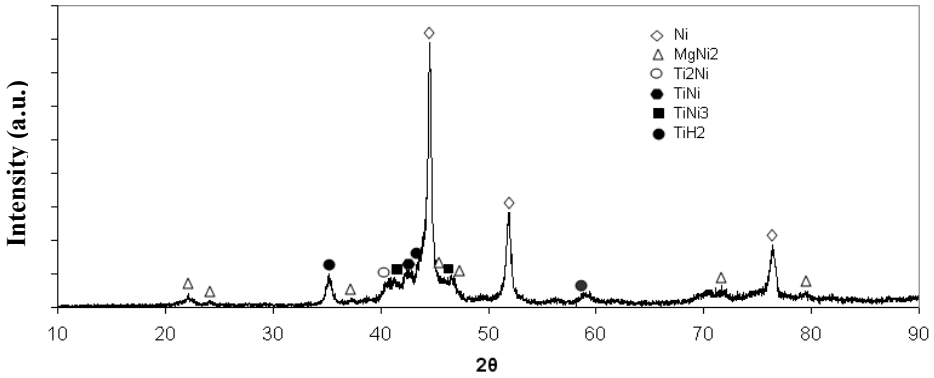

(b)

Figure 4. 23 XRD pattern of (a) hydrided sample, (b) dehydrided sample at 300° C under vacuum.

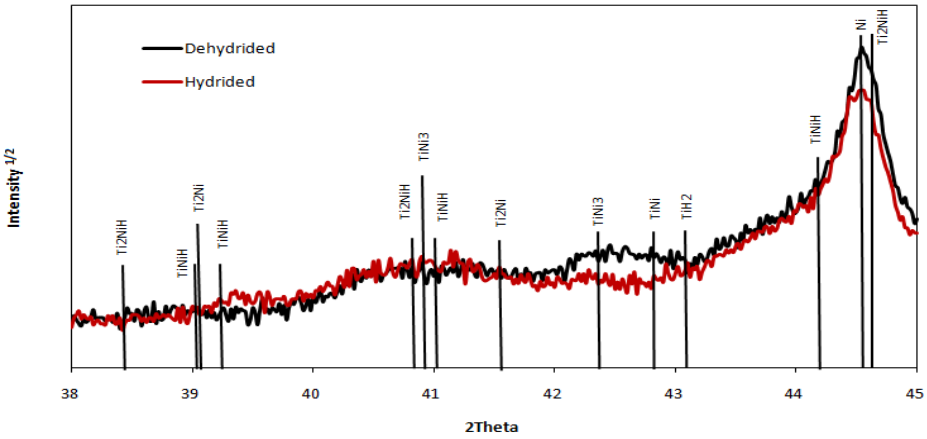

Figure 4. 24 Superimposed XRD patterns of expanded portion of hydrided and dehydrided samples (38° <2θ< 45°) of $MgNi_2$-Ni-Ti.

The expected positions of TiNiH and Ti_2NiH as well as TiNi and Ti_2Ni are marked in this figure. From careful inspection of the patterns, the accumulation of intensities close to 39.26 in hydrided sample, and again similar, more pronounced, broadened accumulation of intensities at $2\theta = 42.80$ in dehydrided sample seem to comply with the presence of TiNiH phase.

In conclusion, as far as Field A (i.e. $MgNi_2$-Ni-Ti) is concerned, the current approach of making use of powders consolidated via heavy ECAP deformation and annealing has successfully yielded the material library comprising the multitude of phases Ti, Ti_2Ni, TiNi, $TiNi_3$, Ni and $MgNi_2$. It should be emphasized that no other phase has been reported for the current triangle, though no study is available for the ternary phase diagram of Mg-Ni-Ti. Screening of the current material library has shown that two phases can store hydrogen: Ti and possibly TiNi.

Screening of Field B (Mg-Ti-$MgNi_2$) was carried in a similar manner. The sample prepared via the powder route was hydrogenated in the Sievert apparatus. Pressure temperature curves are given in Figure 4.25 (a) and (b), for the first and the second hydrogenation cycles. Here, the pressure which was initially at 5 bar deviates from linearity starting from temperatures around 170°C indicating absorption for the first cycle, Figure 4.25 (a). Further increase in temperature leads to partial recovery of pressure at around 320° C and then on the pressure changes linearly below the Ar line.

Pressure temperature curve recorded for the second cycle is given in Figure 4.25 (b). This sample was cooled from 380 °C under vacuum before reloading it with hydrogen. A similar hydrogenation trend was observed, except for the fact that the pressure following its drop recovers to a considerable extent. This implies the presence of a phase that was hydrogenated at the first cycle and its remanence as a hydride in the second cycle. It should also be noted that the temperature range corresponding to a pressure drop shifts to lower values in the

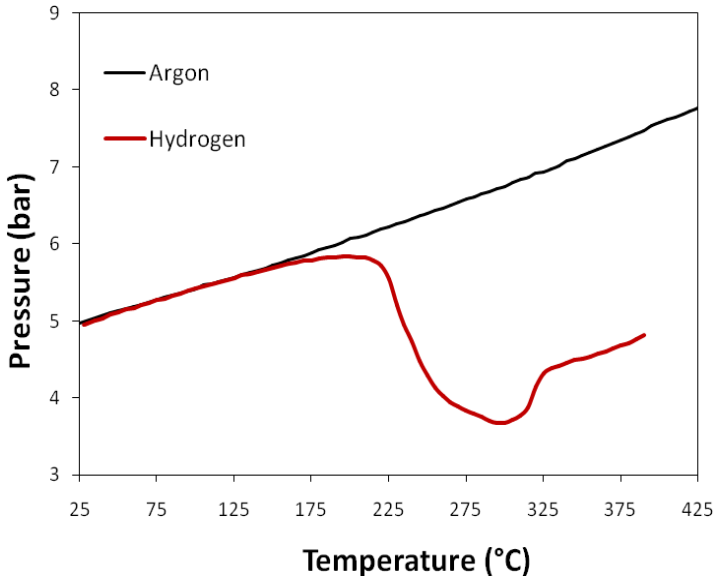

(a)

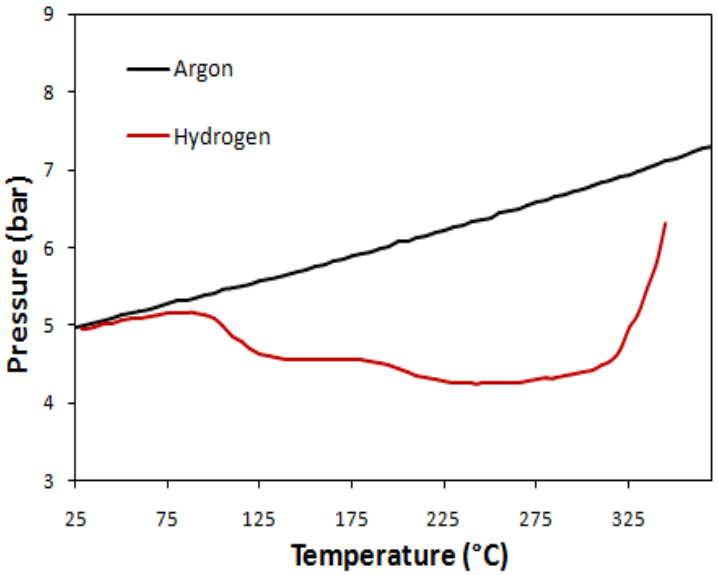

(b)

Figure 4. 25 Pressure-temperature curve for Mg-Ti $MgNi_2$ recorded in a constant volume under hydrogen pressure of approx. 5 bar. Linear variation recorded with Ar is also shown.a) Hydrogenation curve for the first cycle.. b) Hydrogenation curve for the second cycle.

second cycle. Pressure decrease which occured at 170 °C in the first cycle; occurs at 80 °C in the second cycle.

XRD pattern of the sample following the second cycle, cooled under hydrogen from 360 °C is given in Figure 4.26. Phases present are TiH_2, Mg_2NiH_4, Mg, Ni, $MgNi_2$. Figure 4.24 (b) shows XRD pattern of the sample before hydrogenation. Here the phases were Mg_2Ni, $MgNi_2$, Ti, Ni, Mg. Thus hydrogenation affected mainly Ti and Mg2Ni and converted them TiH_2 and Mg_2NiH_4. Following the observation made in Mg-Ni system it appears that the phase which reversibly absorb hydrogen is Mg_2Ni. It appears that TiH_2 forming in the first cycle could not be dehydrogenated under current temperature and vacuum conditions.

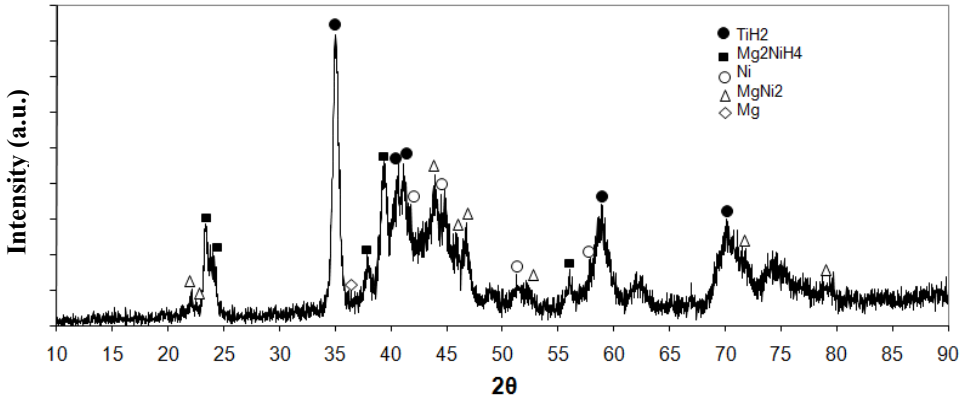

Figure 4. 26 XRD pattern of hydrided $MgNi_2$-Mg-Ti. The hydride phases are Ti and Mg_2Ni.

To sum up, for Field B, the procedure employed which made use of $MgNi_2$-Ti-Mg yielded only one additional Mg_2Ni phase. There is only one report indicating the presence of a ternary compound that falls in Field B (Guanglia et al. 2001). This is Mg_3TiNi_2 which was not observed in the current experiment. Considering the existence of such a phase, the current combinatorial approach used for Field B would be considered to be partially successful.

CHAPTER 5

CONCLUSIONS

A combinatorial method was described for hydrogen storage alloys which involve processes very similar to those normally used in their fabrication. The method makes use of elements or compounds in powder form which are mixed in equal volumetric proportions and then consolidated via methods of severe plastic deformation. The material library was obtained by solid-state reactions of deformed powders brought about by a post annealing treatment. Screening of the material library with respect to their hydrogen storage potentials was achieved with a temperature programmed sorption experiment, combined with the analysis of X-ray data before and after hydrogenation.

The study has shown that success of the method, in the first place, requires the formation of complete library, i.e. the sample should cover all phases relevant to the mixture whether it is binary, ternary or a more complex system. It has been shown that the use of a single sample, though highly desirable, may not be sufficient for yielding all relevant phases, as was shown to be the case for Mg-Ti-Ni. In such cases, a suitable partitioning of alloy systems, i.e. grouping of phases of similar solidus temperatures, would be necessary, using a separate sample for each partition. The usefulness of the current approach in this respect has been illustrated by the formation of six phases side by side in a single sample produced from a powder mixture of $MgNi_2$-Ti-Ni as well as by identification of Mg_2Ni as hydrogen storage composition.

REFERENCES

Aizawa T., Kuji T., Nakano H., *Journals of Alloys and Compounds*, vol. 291 **(1999)**, p. 248-253

Akyıldız H., Çakmak G, Tan S., Öztürk T., 9*th International Symposium on Metal-Hydrogen Systems; Fundamentals and Applications*, Abstracts, Figiel et al (ed.), Cracow Sept.**(2004)**

Akyıldız H., Çakmak G, Tan S., Öztürk T., *Turkish J. Eng. Env. Sci*, vol. 31, (**2007),** p. 289-295

Barkhordarian G., Klassen T., Bormann R., *Journal of Alloys and Compounds*, vol. 364 **(2004)**, p. 242–246

Blomovist H., Noreus D., Babushkin O., Nion F., Vourinen E., *Journal of Materials Science Letters*, vol. 22 **(2003)**, p. 1487-1489

Bobet J.L., Chevalier B., *Intermetallics*, vol. 10 **(2002)**, p. 597–601

Boettcher A. , Haase G., Thun R., Z. Metallk., vol. 46 **(1955),** p. 386

Bogdanovic B., Bohmhammel K., Christ B., Reiser A., Schlichte K.,Vehlen R., Wolf U., Journal of Alloys and Compounds, vol. 282 **(1999),** p. 84–92

Buchner H., *Z. Metallkd*, vol. 63 **(1972)**, p. 497

Buschow K. H., *Solid State Communications*, vol. 17 **(1975)**, p. 891-893

Bystrzycki J., Czujko T., Varin R.A., Oleszak D., Durejko T., Darlewski W., Bojar Z., Przetakiewicz W., *Advanced Materials*, vol. 5 **(2003)**, p. 450-454

Chang H., Yu K-M., Dong Y., Xiang X-D., *Applied Physics Letter*, vol. 81 **(2002)**, p. 2062-2064

Chen C.P., Xu Y.H., Wang X.L., Wang Q.D., *Journal of Power Sources*, vol. 112 **(2002)**, p. 105-108

Cohen-Adad M. Th., Gharbi M., Goutaudier C., Cohen-Adad R., *Journal of Alloys and Compounds*, vol. 289 **(1999)**, p. 185–196

Cullity B.D., *Elements of X-Ray Diffraction*, **(1978)**

Dam B., Gremaud R., Broedersz C., Griessen R., *Scripta Materialia*, vol. 56 **(2007),** p. 853–858

Emiliani M., Richman M., Brown R., *Metallurgical and Materials Transactions A*, vol. 21 (1990), p. 1613-1625

Eskandarany M.S.E., Ahmed H.A., Sumiyama K., Suzuki K., *Journal of Alloys and Compounds*, vol. 218 **(1995)**, p. 36-43

FACT, *Facility for the Analysis of Chemical Thermodynamics*, http://www.crct.polymtl.ca/fact/, **(2008)**

Friedrichs O., Klassen T., Sanchez-Lopez J.C., Bormann R., Fernandez A., *Scripta Materialia***,** vol. 54 **(2006),** p. 1293–1297

Geysen H.M., Meloen R.H., Barteling S.J., *Proc. Nat. Acad. Sci. USA*, vol. 81 **(1984)**, p. 3998-4002

Gremaud R., Broedersz C.P., Borsa D.M., Borgschulte A., Mauron P., Schreuders H., Rector J.H., Dam B., Griessen R., *Advanced Materials*, vol. 19 **(2007)**, p. 2813-2817

Griessen R., Dam B., Gremaud R., Broedersz C., *Scripta Materialia*, vol. 56 **(2007)**, p. 853–858

Guanglia L., Linshen C., Lianbang W., Huantang Y., *Journal of Alloys and Compounds*, vol. 321 **(2001)**, p. L1–L4

Güvendiren M., Baybörü E., Öztürk T., *International Journal of Hydrogen Energy*, vol. 29 **(2004)**, p. 491-496

Hanak JJ., *Journal of Vacuum Science Technology*, vol.8 **(1971)**, p. 172-175

Hasebe M., Nishizawa T., Carter G.C., Application *of Phase Diagrams in Metallurgy and Ceramics*, vol. 2 **(1978)**, p. 911

Hatano Y., Watanabe K., *Materias Transactions*, vol.43 **(2002),** p. 1105-1109

Haussermann U., Blomqvist H., Noreus D., *Inorganic Chemistry*, vol.41 **(2002)**, p. 3684-3692

Hong T.W., Kim Y.J., *Journal of Alloys and Compounds*, vol. 330 **(2002)**, p. 584–589

Huhn P.A., Dornheim M., Klassen T., Bormann R., *Journal of Alloys and Compounds*, vol. 404 **(2005)**, p. 499–502

Imamura H., Tabata S., Shigetomi N., Takesue Y., Sakata Y., *Journal of Alloys and Compounds*, vol. 330 **(2002)**, p. 579–583

Janot R., Aymard L., Rougier A., Nazri G.A., Tarascon J.M., *Journals of Physics and Chemistry of Solids*, vol. 65 **(2004)**, p. 529-534

Jensen T.R., Andreasenb A., Vegge T., Andreasen J.W., Stahl K., Pedersen A.S., Nielsen M.M., Alfons M. M., Besenbacher F., *International Journal of Hydrogen Energy*, vol. 31 **(2006)**, p. 2052-2062

Jin Z., *Scandinavian Journal of Metallurgy*, vol.10 **(1981)**, p. 279-287

Kennedy K., Stefansky T., Davy G., Zackay V.F., Parker E.R., *Journal of Applied Physics*, vol. 36 **(1965)**, p. 3808-3810

Klassen T., Friedrichs O., Sanchez-Lopez J.C., Bormann R., Fernandez A., *Scripta Materialia*,vol. 54 **(2006)**, p. 1293–1297

Kubota H., Takahashi R., Kim T.W., Kawazoe T., Ohtsu M., Arai N., Yoshimura M., Nakao H., Furuya H., Mori Y., Sasaki T., Matsumoto Y., Koinuma H., *Applied Surface Science*, vol. 223 **(2004)**, p. 241–244

Kulikov N. I., *Journal of the Less-Common Metals*, vol. 107 **(1985)**, p. 111-129

Kulkarnı J.S., Kazakova O., Holmes J.D., *Applied Physics A*, vol. 85 **(2006)**, p. 277–286

Kusedome Y., Ikeda K., Nakamori Y., Orimo S., Horita Z., *Scripta Materials*, vol. 57 **(2007)**, p.751-753

Kyoi D., Sato T., Rönnebro E., Kitamura N., Uedac A., Ito M., Katsuyama S., Hara S., Noreus D., Sakai T., *Journal of Alloys and Compounds*, vol. 372 **(2004)**, p. 213–217

Liang G., Huot J., Boily S., Neste A.V., Schulz R., *Journal of Alloys and Compounds*, vol. 282 **(1999),** p. 286–290

Liang G., Huot J., Boily S., Van Neste A., Schulz R., *Journal of Alloys and Compounds*, vol. 292 **(1999)**, p. 247–252

Liang G., Schulz R., *Jornal of Materials Science*, vol. 38 **(2003)**, p. 1179 – 1184

Malov Y.I., Fokin V.N., Troitskaya S.L., Fokina E.E., Shilkin S.P., *Russian Journal of Inorganic Chemistry*, vol. 39 **(1994)**, p. 1712-1714

Massalski T.B., Okamoto H., Subramanian P.R., Kacprzak, L., editors, *Binary alloy phase diagrams*, *2nd edition, vol. 3.* Materials Park, OH, ASM International; (**1990)**, 2874.

Mueller W.M., Blackledge J.P., Libowitz G.G., *Metal Hydrides*, **(1968)**

Manchester F.D., San-Martin A., *Phase Diagrams of Binary Magnesium Alloys*, **(1988)**

Nayeb-Hashemi A.A., Clark J.B., *Bull. Alloy Phase Diagrams* **6**, **(1985)**, 238 - 244.

Nayeb-Hashemi A.A., Clark J.B., editors, *Phase diagrams of Binary Magnesium Alloys*, ASM International, Metals Park, OH, **(1998),** 324-327.

Noreus D., *International Journal of Hydrogen Energy*, vol. 10 **(1985)**, p. 547

Okamoto H., *ASM Handbook Alloys Phase Diagrams,* vol. 3, **(1992)**

Olk H., Tibbetts, G. G. Simon, D. Moleski, J. J., *Journal. Applied.Physichs.vol. 94* **(2003)**, p.720-725.

Orimo S., Fujii H., *Apllied Physichs*, vol. 72 **(2001)**, p. 167-186

Orimo S., Fujii H., *Intermetallics*, vol. 6 **(1997)**, p. 185-192

Palanisamy U.D., Lowe C.R., *Journal of Chromatography A*, vol. 1075 **(2005)**, p. 95–102

Pedersen A.S., Kjoller J., Larsen B., Vigeholm B., *International Journal of Hydrogen Energy*, vol. 8 **(1983)**, p. 205-211

Raab G.I., *Materials Science and Engineering A*, vol. 410 **(2005)**, p. 230–233

Reilly J.J., Wiswall R.H., *Inorganic Chemistry*, vol. 7 **(1968)**, p. 2254-2256

Ronnebro E., Jensen J.O., Noreus D., Bjerrum N.J., *Journal of Alloys and Compounds*, vol. 293 **(1999)**, p. 146–149

Saita I., Li L., Saito K., Akiyama T., *Materials Transactions*, vol. 43 **(2002)**, p. 1100-1104

Schmidt R., Schleret M., Wipf H., Assmus W., Müllner M., *Journal of Physics Condensed Materials*, vol. 1 **(1989),** p. 2473-2482

Schulz R., Huot J,. Liang G., Boily S., Lalande G., Denis M.C., Dodelet J.P., *Material Science Engineering*, vol. 267 **(1999)**, p. 240

Segal V.M., *Material Science Engineering A*, vol. 197 **(1995)**, p. 157-164

Sheppard D.A., Jiang Z.T., Buckley C.E., *International Journals of Hydrogen Energy*, vol. 32 **(2006)**, p. 1928-1932

Song, M.Y. *Journal of Alloys and Compounds* , vol. 282 **(1999)**, p. 297–301

Spassov T., Solsona P., Bliznakov S., Surinach S., Baro M.D., *Journal of Alloys and Compounds*, vol. 356 **(2003)**, p. 639–643

Takahashi R., Yonezawa Y., Ohtani M., Kawasaki M., Matsumoto Y., Koinuma H., *Applied Surface Science*, vol.252 **(2006)**, p. 2477–2481

Takeshita H.T., Tanaka H., Kuriyama N., Sakai T., Uehara I., Haruta M., *Journal of Alloys and Compounds*, vol. 311 **(2000)**, p. 188–193

Takeshita H.T., Tanaka H., Kuriyama N., Kiyobayashi T., Taketichi N., *Journal of Alloys and Compounds*, vol. 330 **(2002)**, p. 517-521

Takeuchi I., Famodu O.O., Read J.C., Aronova M.A., Chang K.S., Craciunescu C., *Nature Materials*, vol. 2 **(2003)**, p. 180

Varin R.A., Czujko T., Wasmund E.B., Wronski Z.S., *Journal of Alloys and Compounds*, vol. 432 **(2007)**, p. 217-231

Vermeulen P., Niessen R.A.H., Notten P.H.L., *Electrochemistry Communications*, vol. 8 **(2006)**, p. 27 –32

Vermeulen P., Thiel E. F. M. J., Notten P.H.L., *Chemistry European Journal*, vol. 13 **(2007)**, p. 9892 – 9898

Vijaya R., Sundaresana R., Maiyab M.P., Murthy S.S., *International Journal of Hydrogen Energy*, vol. 30 **(2005)**, p. 501-508

Xiang X-D., Sun X, Briceno G., LouY., Wang K., Chang H., Wallace-Freedom W-G., Chen S-W., Schultz P.G., *Science*, vol. 268 **(1995)**, p. 1738- 1740

Yang H., Yuan H, Ji J., Sun H., Zhou Z., Zhang Y., *Journal of Alloys and Compounds*, vol. 330 **(2002)**, p. 640–644

Yang S., Julian R., Evans G., *Materials Science and Engineering A*, vol. 379 **(2004)**, p. 351–359

Yermakov A.Y., Mushnikov N.V., Uimin M.A., Gaviko V.S, Tankeev A.P., Skripov A.V., Soloninin A.V., Buzlukov A.L., *Journal of Alloys and Compounds*, vol. 425 **(2006)**, p. 367–372

Yvon K., Schefer J., Stuckıic I.F., *Inorganic Chemistry*, vol. 20 **(1981)**, p. 2776-2778

Zaluska A., Zaluski L. Ström-Olsen J.O., *International Application* No:PCT/CA1998/000947, IPC:C01B 3/00, Pub. No. :WO/2000/020329, **(2006)**

Zaluska A., Zaluski L., Strom–Olsen J.O., *Journal of Alloys and Compounds*, vol. 288 **(1999)**, p. 217–225

Zhao J.C., Lemmon J.P., Smentkowski V.S., 9*th International Symposium on Metal-Hydrogen Systems; Fundamentals and Applications*, Abstracts, Figiel et al (ed.), Cracow Sept, **(2004)**

Zhao J-C., *Advanced Engineering Material*, vol. 3 **(2001)**, p. 143

Zhao J-C., *Material Research*, vol. 16 **(2001)**, p. 1565

Zhao J-C., *Progress in Material Science*, vol. 51 **(2006)**, p. 557-631